









ARTICLE

Excitation–Contraction Coupling

Calcium current modulation by the γ_1 subunit depends on alternative splicing of $\text{Ca}_v1.1$

Yousra El Ghaleb¹, Nadine J. Ortner² , Wilfried Posch³, Monica L. Fernández-Quintero⁴, Wietske E. Tuinte¹ , Stefania Monteleone⁴, Henning J. Draheim⁵ , Klaus R. Liedl⁴, Doris Wilflingseder³ , Jörg Striessnig² , Petronel Tuluc² , Bernhard E. Flucher¹ , and Marta Campiglio¹ 

The skeletal muscle voltage-gated calcium channel ($\text{Ca}_v1.1$) primarily functions as a voltage sensor for excitation–contraction coupling. Conversely, its ion-conducting function is modulated by multiple mechanisms within the pore-forming α_{1S} subunit and the auxiliary $\alpha_2\delta-1$ and γ_1 subunits. In particular, developmentally regulated alternative splicing of exon 29, which inserts 19 amino acids in the extracellular IVS3–S4 loop of $\text{Ca}_v1.1a$, greatly reduces the current density and shifts the voltage dependence of activation to positive potentials outside the physiological range. We generated new HEK293 cell lines stably expressing $\alpha_2\delta-1$, β_3 , and STAC3. When the adult ($\text{Ca}_v1.1a$) and embryonic ($\text{Ca}_v1.1e$) splice variants were expressed in these cells, the difference in the voltage dependence of activation observed in muscle cells was reproduced, but not the reduced current density of $\text{Ca}_v1.1a$. Only when we further coexpressed the γ_1 subunit was the current density of $\text{Ca}_v1.1a$, but not that of $\text{Ca}_v1.1e$, reduced by >50%. In addition, γ_1 caused a shift of the voltage dependence of inactivation to negative voltages in both variants. Thus, the current-reducing effect of γ_1 , unlike its effect on inactivation, is specifically dependent on the inclusion of exon 29 in $\text{Ca}_v1.1a$. Molecular structure modeling revealed several direct ionic interactions between residues in the IVS3–S4 loop and the γ_1 subunit. However, substitution of these residues by alanine, individually or in combination, did not abolish the γ_1 -dependent reduction of current density, suggesting that structural rearrangements in $\text{Ca}_v1.1a$ induced by inclusion of exon 29 may allosterically empower the γ_1 subunit to exert its inhibitory action on $\text{Ca}_v1.1$ calcium currents.

Introduction

Excitation–contraction (EC) coupling in skeletal muscle is initiated by action potentials that activate the voltage-gated calcium channel $\text{Ca}_v1.1$ located in the transverse tubules (T-tubules). In adult skeletal muscle, $\text{Ca}_v1.1$ functions as a voltage sensor that triggers the opening of the calcium release channel, the ryanodine receptor (RyR1), in the SR via protein–protein interactions, thus initiating muscle contraction (Rios and Brum, 1987; Schneider and Chandler, 1973). Because of the conformational coupling between $\text{Ca}_v1.1$ and RyR1, $\text{Ca}_v1.1$ currents are dispensable for skeletal muscle EC coupling (Armstrong et al., 1972; Dayal et al., 2017). Accordingly, in mammals, $\text{Ca}_v1.1$ channels activate only upon strong, non-physiological membrane depolarization and conduct small and slowly activating currents (Tanabe et al., 1988). This is strikingly different in the embryonic splice variant ($\text{Ca}_v1.1e$), which lacks 19 amino acids in the extracellular loop connecting segments S3 and S4 in the

fourth homologous repeat, owing to alternative splicing excluding exon 29 (Tuluc et al., 2009). The embryonic $\text{Ca}_v1.1e$ isoform activates upon physiological membrane depolarization and conducts currents that are substantially larger in amplitude than those of the adult $\text{Ca}_v1.1a$ isoform.

$\text{Ca}_v1.1$ is a multiprotein complex consisting of a pore-forming α_1 subunit and several auxiliary proteins: the intracellular β_{1a} , the glycosylphosphatidylinositol-anchored extracellular $\alpha_2\delta-1$, and the transmembrane γ_1 subunits (Curtis and Catterall, 1984; Zamponi et al., 2015). While the β_{1a} subunit was shown to be essential for the functional expression of $\text{Ca}_v1.1$ and for EC coupling (Gregg et al., 1996; Schredelseker et al., 2005), $\alpha_2\delta-1$ and γ_1 are dispensable for functional expression of $\text{Ca}_v1.1$ in muscle cells but displayed an inhibitory effect on $\text{Ca}_v1.1$ currents (Freise et al., 2000; Obermair et al., 2005; Held et al., 2002; Ursu et al., 2001; Arikath et al., 2003; Tuluc et al., 2009; Ahern et al.,

¹Institute of Physiology, Department of Physiology and Medical Physics, Medical University Innsbruck, Innsbruck, Austria; ²Department of Pharmacology and Toxicology, Center for Molecular Biosciences Innsbruck, University of Innsbruck, Innsbruck, Austria; ³Institute of Hygiene and Medical Microbiology, Medical University of Innsbruck, Innsbruck, Austria; ⁴Institute of General, Inorganic and Theoretical Chemistry, University of Innsbruck, Innsbruck, Austria; ⁵Boehringer Ingelheim Pharma GmbH & Co KG, CNS Research, Biberach an der Riss, Germany.

Correspondence to Bernhard E. Flucher: bernhard.e.flucher@i-med.ac.at; Marta Campiglio: marta.campiglio@i-med.ac.at

Stefania Monteleone's present address is Evotec (UK) Ltd., Abingdon, UK. This work is part of a special issue on excitation–contraction coupling.

© 2022 El Ghaleb et al. This article is available under a Creative Commons License (Attribution 4.0 International, as described at <https://creativecommons.org/licenses/by/4.0/>).

2001). The $\alpha_2\delta$ -1 subunit slows down the kinetics of activation of $\text{Ca}_v1.1$ currents, whereas the γ_1 subunit reduces the current amplitude and shifts the voltage dependence of inactivation. However, neither the $\alpha_2\delta$ -1 nor the γ_1 subunit is essential for EC coupling. In their absence, the amplitude and voltage dependence of the depolarization-induced calcium transients are unchanged (Obermair et al., 2005; Ahern et al., 2001; Ursu et al., 2004).

All the cited studies were performed in skeletal muscle cells using a knockout or knockdown approach since $\text{Ca}_v1.1$ expresses poorly in mammalian non-muscle cells. Whereas coexpression of the auxiliary subunits β and $\alpha_2\delta$ is sufficient to support functional expression of all other high voltage activated calcium channels (Singer et al., 1991; Lacerda et al., 1991; Zamponi et al., 2015), $\text{Ca}_v1.1$ coexpression with these subunits does not yield functional currents in heterologous cell systems. Only recently, it was demonstrated that the skeletal muscle-specific adaptor protein STAC3 is essential for membrane expression and robust currents of $\text{Ca}_v1.1$ in heterologous cells (Polster et al., 2015; Wu et al., 2018).

In the present study, we generated two HEK cell lines stably expressing the three subunits (STAC3, β_3 , and $\alpha_2\delta$ -1) necessary to support functional membrane expression of $\text{Ca}_v1.1$. These cell lines provide a unique tool for analysis of wild type and mutant $\text{Ca}_v1.1$ channel currents and pharmacology in non-muscle cells. Interestingly, in contrast to what had been reported in myotubes, our current analysis of the adult and embryonic $\text{Ca}_v1.1$ splice variants in the STAC3-HEK cell lines revealed no difference in their current densities, but still displayed the typical differences in voltage dependence of activation. Because coexpression of γ_1 inhibits gating of $\text{Ca}_v1.1a$ calcium currents in skeletal myotubes and tsA201 cells (Polster et al., 2016; Freise et al., 2000; Ahern et al., 2001), and because the recently resolved $\text{Ca}_v1.1$ structure revealed an interaction of γ_1 subunit with the IVS3-S4 loop of $\text{Ca}_v1.1a$ (Wu et al., 2016; Wu et al., 2015), we hypothesized that regulation of the gating properties of $\text{Ca}_v1.1$ channels by the γ_1 subunit occurs in a splice variant-dependent manner. Indeed, we found that coexpressed γ_1 subunits selectively reduced the current density of the adult $\text{Ca}_v1.1a$ isoform, and not that of the embryonic $\text{Ca}_v1.1e$ isoform. In contrast, γ_1 similarly shifted the voltage dependence of steady-state inactivation to more negative voltages and increased $\text{Ca}_v1.1$ membrane expression of both isoforms. Molecular modeling predicted several ionic interactions between the γ_1 subunit and the IVS3-S4 linker of $\text{Ca}_v1.1a$. However, site-directed mutagenesis of the putative ion-pair partners did not abolish γ_1 -dependent inhibition of the $\text{Ca}_v1.1a$ currents, suggesting an allosteric effect of exon 29 that is important for modulation of current density by the γ_1 subunit.

Materials and methods

Generation of stable cell lines

Two HEK293 cell lines stably expressing mouse STAC3 were generated using the Flp-In T-Rex system (Invitrogen). Host cells, already expressing human $\alpha_2\delta$ -1 and β_3 subunits and containing a flippase recognition target (FRT) site, allowed the integration

of STAC3 into the genome in a Flp recombinase-dependent manner. Briefly, the coding sequence of mouse STAC3 (Q8BZ71) was cloned into the pTO-HA-strepIII C GW FRT vector (containing an FRT site and a hygromycin resistance gene). To generate the cell line constitutively expressing STAC3 (HEK-STAC3), STAC3 expression was under the control of a CMV promoter. To generate the inducible STAC3 expression cell line (HEK-TetOn-STAC3), STAC3 expression was under the control of a CMV promoter with a tetracycline operator (TetOn) element. HEK293 host cells were transfected using the calcium phosphate method with either plasmid or a Flp recombinase-expressing vector (pOG44). Subsequently cells were selected with hygromycin B (50 $\mu\text{g}/\text{ml}$; cat. #CP12.2; Lactan/Roth) and selection agents for the other subunits (see below), and single-positive cell clones were propagated and characterized. The electrophysiological experiments for the characterization of the cell lines were carried out using the TetOn-STAC3 cell line (Figs. 3, 4, 6, and S1).

Although the cell lines contain the β_3 isoform, rather than the skeletal muscle-specific β_{1a} , no drawbacks are expected when expressing a non-muscle β subunit in non-muscle cells. Accordingly, the cell lines expressing β_3 efficiently supported robust $\text{Ca}_v1.1$ currents (Fig. 2). Also, because we compared differences due to splicing or γ_1 coexpression (mostly involving the transmembrane or extracellular part of the channel), the type of the intracellular β subunit is not expected to affect our current analysis.

Cell culture and transfection

Cells were cultured in DMEM (cat. #41966052; Invitrogen) supplemented with 10% FBS (F9665; Sigma-Aldrich), 2 mM L-glutamine (25030-032; Invitrogen), and 10 U/ml penicillin-streptomycin (15140122; Invitrogen) and were maintained at 37°C in a humidified incubator with 5% CO_2 . For maintenance of the stable cell lines, selection agents for each subunit were applied regularly (STAC3, 50 $\mu\text{g}/\text{ml}$ hygromycin B; β_3 , 500 $\mu\text{g}/\text{ml}$ geneticin [10131035; Gibco]; and $\alpha_2\delta$ -1, 15 $\mu\text{g}/\text{ml}$ blasticidin S [A1113903; Gibco]).

For electrophysiological experiments, cells were plated on 35-mm dishes coated with poly-L-lysine (cat. #P2636; Sigma-Aldrich) and simultaneously transfected with 2 μg of DNA using Eugene HD (cat. #E2312; Promega), according to the manufacturer's instructions. For the TetOn cell line, STAC3 expression was induced using 1 $\mu\text{g}/\text{ml}$ doxycycline (DOX) upon transfection (cat. #3072; Sigma-Aldrich), and cells were kept at 5% CO_2 and 30°C. Cells were used for patch-clamp experiments 24–48 h after transfection/induction.

Plasmids

Cloning procedures for GFP- $\text{Ca}_v1.1a$ and GFP- $\text{Ca}_v1.1e$ were previously described (Grabner et al., 1998; Tuluc et al., 2009). Mouse γ_1 was cloned from genomic cDNA from mouse soleus muscle. Primer sequences were selected according to GenBank NM-007582. Briefly, the cDNA of γ_1 was amplified by PCR with a forward primer introducing a KpnI site upstream the starting codon (5'-ATATGGTACCATGTACACAGACCAAAACAGCGAAG-3') and the reverse primer introducing a SalI site after the stop codon (5'-ATATGTCGACGCTAGTGCTCTGGCTCAGCGTCCATG

CA-3'). After EcoRI/ApaI digestion, the PCR fragment obtained was inserted into the KpnI/XhoI-digested pcDNA3 vector, yielding pcDNA3- γ_1 .

The 13-residue bungarotoxin (BTX) binding site (BBS) was inserted in the IIS5-S6 loop of Ca_v1.1a or Ca_v1.1e at residue 593 by overlap extension PCR. Briefly, the cDNA sequence of Ca_v1.1 was amplified with overlapping primers in separate PCR reactions using GFP-Ca_v1.1a as template. Primers used for the first fragment were forward, 5'-TACATGAGCTGGATCAG-3', and reverse, 5'-GTAGGGCTCCAGGGAGCTCTCGTAGTATCTCCAGTGTGCGACTTCCGTGTCTCGAAGTC-3'. Primers used for the second fragment were forward, 5'-TACGAGAGCTCCCTGGAGCCC TACCCTGACGTACGTTGAGGACACGGAAGTGCACGC-3', and reverse, 5'-GAACACGCACTGGACCACG-3'. The two separate PCR products were then used as template for a final PCR reaction with flanking primers to connect the nucleotide sequences. The resulting PCR fragment was EcoRI/XhoI digested and inserted into EcoRI/XhoI-digested GFP-Ca_v1.1a or GFP-Ca_v1.1e, yielding GFP-Ca_v1.1a-BBS or GFP-Ca_v1.1e-BBS.

The R160A mutation was introduced by overlap extension PCR. Briefly, the cDNA sequence of γ_1 was amplified with overlapping primers mutating R160 into an alanine in separate PCR reactions using pcDNA3- γ_1 as template. Primers used for the first fragment were forward, 5'-ATATGGTACCATGTACA GACCAAAACAGCGAAG-3', and reverse, 5'-CACCGACTGCGC CATGACCTCCACGGAGACGATGAG-3'. Primers used for the second fragment were forward, 5'-GAGGTCATGGCGCAGTCG GTGAAGCGTATGATTGAC-3', and reverse, 5'-ATATGTGCAGC CTAGTGCTCTGGCTCAGCGTCCATGCA-3'. The two separate PCR products were then used as template for a final PCR reaction with flanking primers to connect the nucleotide sequences. The resulting PCR fragment was KpnI/SalI digested and inserted into the KpnI/XhoI-digested pcDNA3 vector, yielding pcDNA3- γ_1 -R160A.

The K102A and E103A mutations were introduced by PCR. Briefly, the cDNA sequence of γ_1 (nt 288–672) was amplified by PCR with a forward primer introducing the K102A and the E103A mutations downstream of the EcoRI site and the reverse primer introducing an ApaI site after the stop codon. Primers used were forward, 5'-TGAATTCACCACTCAAGCGGCGTACAG CATCTCAGCAGCGGCCATT-3', and reverse, 5'-AGAATAGGG CCCCCCTCGACGCT-3'. After EcoRI/ApaI digestion, the PCR fragment obtained was inserted into the EcoRI/ApaI-digested pcDNA3- γ_1 vector, yielding pcDNA3- γ_1 -K102A-E103A. To combine the three mutations, we introduced the K102A and E103A mutations as described above, but using γ_1 -R160A as template for the PCR, yielding γ_1 -R160A-K102A-E103A (γ_1 -RKE AAA). Sequence integrity of all newly generated constructs was confirmed by sequencing (MWG Biotech).

RT-PCR

RNA was isolated from the three HEK293 cell lines after 48 h in culture using the RNeasy Protect Mini Kit (cat. #74124; Qiagen). After reverse transcription (Super-Script II reverse transcriptase, cat. #18064022; Invitrogen), the absolute number of transcripts in each sample was assessed by quantitative TaqMan PCR (Mm01159196_m1; Thermo Fisher Scientific), using a standard curve generated from known concentrations of a PCR product

containing the target of the assay as described previously (Rufenach et al., 2020).

Western blotting

Proteins isolated from the three HEK cell lines were prepared as previously described (Campiglio and Flucher, 2017). Briefly, cells plated in 100-mm dishes were trypsinized after 48 h in culture. Cells were lysed in radioimmunoprecipitation assay buffer with a pestle and left on ice for 30 min. The lysates were then centrifuged for 10 min. The protein concentration was determined using a BCA assay (cat. #23250; Pierce). 20 μ g of protein samples were loaded on a NuPage gel (4–12% polyacrylamide, cat. #NP0321; Invitrogen) and separated by SDS-PAGE at 160 V. The protein samples were then transferred to a PVDF membrane at 25 V and 100 mA for 3 h at 4°C with a semidry blotting system (Roth). The membrane was then cut and incubated with rabbit anti-STAC3 (1:2,000; cat. #20392-1; Proteintech; RRID:AB_10693618) or mouse anti-GAPDH (1:100,000; cat. #sc-32233, Santa Cruz Biotechnology; RRID:AB_627679) antibodies overnight at 4°C and then with HRP-conjugated secondary antibody (1:5,000; Pierce) for 1 h at room temperature. The chemiluminescent signal was developed with ECL Supersignal WestPico kit (cat. #34579; Thermo Fisher Scientific) and detected with ImageQuant LAS 4000.

Immunocytochemistry

The three HEK cell lines were plated on poly-L-lysine-coated coverslips and fixed in paraformaldehyde at room temperature after 2 d in culture. Fixed cells were incubated in 5% normal goat serum in PBS/BSA/Triton for 30 min. The rabbit anti-STAC3 antibody (1:2,000) was applied overnight at 4°C and detected with Alexa Fluor 594-conjugated secondary antibody. During the last washing step, cells were incubated with Hoechst dye to stain nuclei. Preparations were analyzed on an Axioimager microscope (Carl Zeiss) using a 63 \times , 1.4-NA objective. Images were recorded with a cooled charge-coupled device camera (SPOT; Diagnostic Instruments) and Metamorph image processing software (Universal Imaging). Images were arranged in Adobe Photoshop CS6 (Adobe Systems), and linear adjustments were performed to correct black level and contrast. To quantify the fluorescence intensity of the STAC3 staining, 14-bit grayscale images of the red (STAC3) and blue (Hoechst) channels were acquired for each cell line. A region of interest was manually traced around each cell in the STAC3 staining image, and its intensity was recorded and background corrected using Metamorph. For each condition, between 15 and 31 cells were analyzed from each of three independent experiments.

Labeling of cell surface Ca_v1.1 channels with QD₆₅₅

For cell-surface labeling, a 13-amino acid high-affinity BBS was inserted into Ca_v1.1a and Ca_v1.1e as described (Yang et al., 2010) and expressed in HEK-293 cells. 48 h after transfection, cells were resuspended from 35-mm dishes with ice-cold PBS⁺⁺ containing calcium and magnesium (pH 7.4, 0.9 mM CaCl₂, and 0.49 mM MgCl₂), washed, and incubated with 5 μ M biotinylated α -BTX (cat. #B1196; Invitrogen) in PBS⁺⁺/3% BSA in the dark for 1 h on ice. Cells were washed twice with PBS⁺⁺/3% BSA and incubated with 10 nM streptavidin-conjugated quantum dots

(QD₆₅₅; cat. #Q10121MP; Invitrogen) in the dark for 1 h on ice. Finally, cells were washed twice with PBS⁺⁺/3% BSA and either assayed by flow cytometry or plated on poly-L-lysine-coated coverslips and imaged.

Microscopy

Cells were mounted in Tyrode's physiological solution and imaged using a 63×, 1.4-NA objective Axioimager microscope (Carl Zeiss). 14-bit images were recorded with a cooled charge-coupled device camera (SPOT; Diagnostic Instruments) and Metaview image processing software (Universal Imaging). Image composites were arranged in Adobe Photoshop CS6.

Multiparameter flow cytometry

Labeled cells were counted by flow cytometry using a BD FACSVerser analyzer. For flow cytometric analyses, labeled cells were counted and analyzed using BD FACSuite v1.0.6 and BD FACS Diva v9.0 software. Cells expressing GFP were excited at 488 nm, and red signal was excited at 633 nm. Our gating strategy assured that the same cell population in terms of size and granularity was counted in each condition. In each set of experiments, untransfected or unlabeled cells, as well as single-color controls, were used to adjust threshold values, and these settings were then used when analyzing all samples.

Electrophysiology

Calcium currents in HEK cells were recorded with the whole-cell patch-clamp technique in voltage-clamp mode using an Axopatch 200A amplifier (Axon Instruments). Patch pipettes (borosilicate glass; Science Products) had resistances between 1.8 and 4.0 MΩ when filled with (in mM) 135 CsCl, 1 MgCl₂, 10 HEPES, 10 EGTA, and 4 ATP-Na₂ (pH 7.4 with CsOH). The extracellular bath solution contained (in mM) 15 CaCl₂, 150 choline-chloride, 10 HEPES, and 1 Mg-Cl₂ (pH 7.4 with CsOH). Data acquisition and command potentials were controlled by pCLAMP software (Clampex version 10.2; Axon Instruments); analysis was performed using Clampfit version 10.7 (Axon Instruments) and SigmaPlot version 12.0 (SPSS Science) software. The current-voltage dependence of activation was determined using 300- or 500-ms-long square pulses to various test potentials (holding potential −80 mV), and curves were fitted according to

$$I = G_{\max} \times (V - V_{\text{rev}}) / \{1 + \exp[-(V - V_{1/2})/k]\},$$

where G_{\max} is the maximum conductance, V_{rev} is the extrapolated reversal potential, $V_{1/2}$ is the potential for half-maximal activation, and k is the slope factor. The conductance was calculated using $G = -I / (V_{\text{rev}} - V)$, and its voltage dependence was fitted according to a Boltzmann distribution:

$$G = G_{\max} / \{1 + \exp[-(V - V_{1/2})/k]\},$$

Steady-state inactivation was calculated as the ratio between two current amplitudes elicited by 200-ms pulses to V_{\max} separated by a 45-s conditioning pulse to various test potentials (sweep start-to-start interval 30 s, time gap between the prepulse and the test pulse 10 ms; see Fig. 4 A, inset). Steady-state inactivation curves were fitted using a modified Boltzmann equation:

$$I = (1 - I_{\text{residual}}) / \{1 + \exp[(V - V_{1/2})/k]\} + I_{\text{residual}},$$

where $V_{1/2}$ is the half-maximal inactivation voltage and k is the inactivation slope factor and I_{residual} is the residual fractional current.

Statistical analysis

All experimental groups were analyzed in transiently transfected cells from at least three independent cell passages/transfections. The means, SEM, and P values were calculated using Student's *t* test, two-tailed, with significance criteria as follows: *, $P < 0.05$; **, $P < 0.01$; ***, $P < 0.001$; and ****, $P < 0.0001$. P values of the experiments in which more than two groups were compared to each other were calculated using ANOVA and Tukey's or Sidak's post-hoc test. The software used for statistical analysis was GraphPad Prism v9.

Structure modeling

The complex structures of both splice variants of the human $\alpha 1$ -subunit (Ca_v1.1e and Ca_v1.1a) and the $\gamma 1$ -subunit were modeled based on the rabbit cryo-EM structure of Ca_v1.1 in the inactivated state, with voltage sensors in the "up" conformation and a closed intracellular gate (PDB accession no. 5GJV; Wu et al., 2016). Homology modeling has been performed using MOE (Molecular Operating Environment, version 2018.08; Molecular Computing Group). Additionally, ab initio Rosetta modeling was used to generate structures for loops that were not resolved in the original Ca_v1.1 $\alpha 1$ -subunit and $\gamma 1$ -subunit template (Rohl et al., 2004). The structures for the putative mutants were derived from both WT splice variant models by replacing the mutated residue and carrying out a local energy minimization using MOE. The C-terminal and N-terminal parts of each domain were capped with acetylamide and *N*-methylethylamide to avoid perturbations by free charged functional groups. The structure model was embedded in a plasma membrane consisting of POPC (1-palmitoyl-2-oleoyl-sn-glycero-3-phosphocholine) and cholesterol in a 3:1 ratio, using the CHARMM-GUI Membrane Builder (Lee et al., 2019; Jo et al., 2009). Water molecules and 0.15 M KCl were included in the simulation box. Energy minimizations of Ca_v1.1e and Ca_v1.1a WT and mutant structures in the membrane environment were performed. The topology was generated with the LEaP tool of AmberTools18 (Case et al., 2008), using force fields for proteins (ff14SBonlisc) and lipids (Lipid14; Dickson et al., 2014). The structure models were heated from 0 to 300°K in two steps, keeping the lipids fixed, and then equilibrated over 1 ns. Molecular dynamics simulations were performed for 10 ns, with time steps of 2 fs, at 300°K and in anisotropic pressure scaling conditions. Van der Waals and short-range electrostatic interactions were cut off at 10 Å, whereas long-range electrostatics were calculated by the particle mesh Ewald method (Salomon-Ferrer et al., 2013). As extracellular loop 1 was not resolved in the cryo-EM structure, we modeled 100 loop structures with Rosetta ab initio modeling (Rohl et al., 2004). By clustering on the loops using an RMSD distance criterion of 2 Å, we obtained 10 clusters. These 10 clusters were carefully evaluated, and the two energetically most favorable cluster representatives, which formed interactions

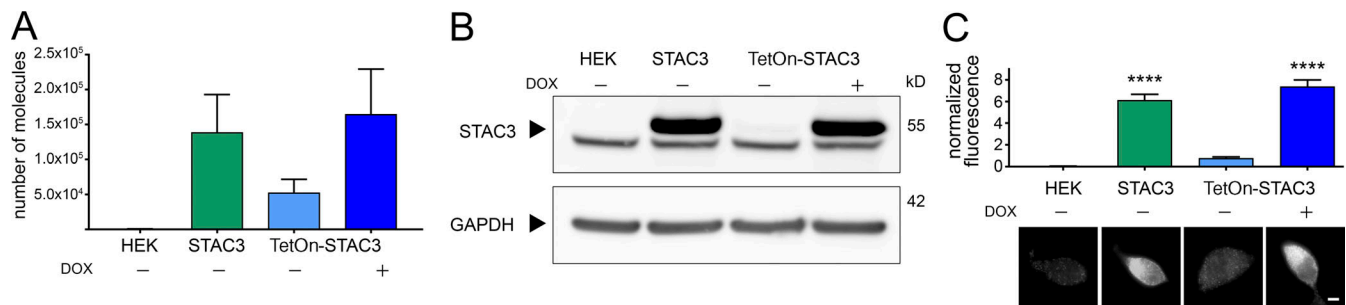


Figure 1. Both the constitutive and the inducible STAC3-HEK cell lines robustly express STAC3. (A) STAC3 mRNA transcription levels in the host (HEK), the constitutive (STAC3), and the inducible (TetOn-STAC3) cell line, before and after DOX treatment, assessed by TaqMan quantitative PCR. Mean values of three replicates. (B) Western blot analysis with anti-STAC3 antibody indicated that STAC3 is substantially expressed by the constitutive and inducible cell lines (treated with DOX), while it is absent from the host cell line (HEK). Without DOX, the inducible cell line shows very low basal expression. An unspecific band present in all samples migrates slightly faster than STAC3. One representative experiment of three is shown. (C) Quantification of STAC3 staining intensity in the host (HEK), the constitutive (STAC3), and the inducible cell line (TetOn-STAC3), before and after DOX treatment reveals strong STAC3 expression in both STAC3 and TetOn-STAC3 cell lines. Scale bar, 2 μ m. ANOVA, $F(3,169) = 67.72$; $P < 0.0001$; Tukey post hoc analysis; ****, $P < 0.0001$. Source data are available for this figure: SourceData F1.

with the S3-S4 loop of VSD IV (exon 29), were considered for further minimizations in the membrane environment. MOE and Pymol were used to visualize the key interactions and point out differences in structure models (The PyMOL Molecular Graphics System; version 2.0, Schrödinger, LLC).

Online supplemental material

Fig. S1 shows the activation and inactivation kinetics analysis pertaining to Fig. 3 (activation) and Fig. 4 (inactivation).

Results

Generation of two HEK cell lines expressing β_3 , $\alpha_2\delta$ -1, and STAC3

In order to generate HEK293 cell lines that could reliably support $\text{Ca}_v1.1$ expression, we inserted STAC3 into the genome of a host cell line already available, stably expressing $\alpha_2\delta$ -1 and β_3 , using the Flp-In T-Rex system. We generated two cell lines: one in which the expression of STAC3 was constitutive (HEK-STAC3) and one in which the expression of STAC3 was DOX inducible (HEK-TetOn-STAC3). While the parental HEK293 cell line showed neither STAC3 mRNA nor protein expression, the selected clone of the constitutive HEK-STAC3 cell line strongly expressed STAC3 (Fig. 1). As expected, without DOX induction, the selected clone of the inducible HEK-TetOn-STAC3 cell line showed only weak basal STAC3 mRNA and protein expression. However, 24 h after the beginning of DOX induction, STAC3 expression levels were strongly increased and comparable to those of the constitutive HEK-STAC3 cell line (Fig. 1).

We then analyzed the ability of the cell lines to support the expression of functional $\text{Ca}_v1.1$ currents by transient transfection with the adult $\text{Ca}_v1.1a$ or the embryonic $\text{Ca}_v1.1e$ isoforms. The two $\text{Ca}_v1.1$ isoforms differ in the length of the linker connecting helices S3 and S4 of the fourth homologous repeat, with the embryonic isoform skipping exon 29 and lacking 19 amino acids. Although both isoforms support skeletal muscle EC coupling, they display very different current properties when expressed in dysgenic ($\text{Ca}_v1.1$ -null) myotubes. In contrast to the adult $\text{Ca}_v1.1a$

isoform, the embryonic $\text{Ca}_v1.1e$ splice variant activates at more hyperpolarizing potentials and conducts calcium currents that are several-fold larger than those of $\text{Ca}_v1.1a$ (Tuluc et al., 2009). Our experiments show that both the constitutive (HEK-STAC3) and the inducible (HEK-TetOn-STAC3) cell lines efficiently supported functional expression of both the adult and the embryonic $\text{Ca}_v1.1$ variants (Fig. 2, A, B, E, and F; and Table 1). More interestingly, while the two $\text{Ca}_v1.1$ splice variants displayed the expected difference in the $V_{1/2}$ of activation (Fig. 2, C, D, G, and H; and Table 1), the expected smaller current density in $\text{Ca}_v1.1a$ was not observed in the two STAC3-HEK cell lines (Fig. 2, A, B, E, and F; and Table 1).

We reasoned that some factor is missing in HEK cells that specifically mediates the splicing-dependent effect on the current amplitude in muscle cells. In muscle, the specific function of exon 29 is to curtail the calcium currents, and in our STAC3-HEK cells the currents were equally large, so the missing factor might be a muscle-specific protein capable of diminishing $\text{Ca}_v1.1$ currents specifically in the adult splice variant. The only $\text{Ca}_v1.1$ subunit not present in our expression system is the γ_1 subunit. Moreover, the γ_1 subunit acts as a negative regulator of $\text{Ca}_v1.1$ currents both in skeletal muscle and in tsA201 cells (Freise et al., 2000; Ahern et al., 2001; Andronache et al., 2007; Polster et al., 2016), and its expression is restricted to skeletal muscle (Biel et al., 1991; Jay et al., 1990). Therefore, we inferred that the γ_1 subunit may be the missing factor selectively reducing the currents of $\text{Ca}_v1.1a$ and not those of $\text{Ca}_v1.1e$. This notion was further supported by the fact that cryo-EM structures of $\text{Ca}_v1.1$ predicted an interaction of the γ_1 subunit with the $\text{Ca}_v1.1$ IVS3-S4 region, exactly the site containing the alternatively spliced exon 29 (Wu et al., 2015, 2016).

The γ_1 subunit selectively reduces the current density of $\text{Ca}_v1.1a$ but not that of $\text{Ca}_v1.1e$

To test this hypothesis, we measured the calcium current density of $\text{Ca}_v1.1a$ and $\text{Ca}_v1.1e$ in the presence and the absence of γ_1 in one of the newly established cell lines (HEK-TetOn-STAC3). As previously reported (Polster et al., 2016; Freise et al., 2000), the presence of γ_1 significantly reduced $\text{Ca}_v1.1a$ current amplitudes, with no significant effect on the voltage dependence of

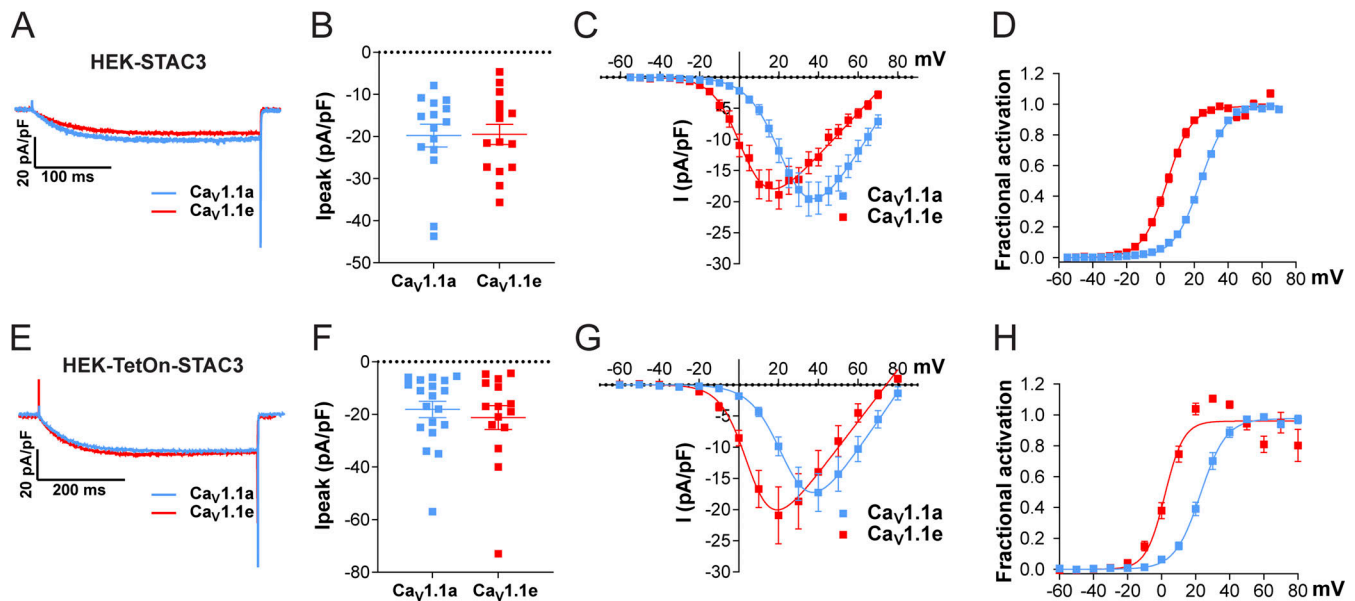


Figure 2. Exclusion of exon 29 in $\text{Ca}_v1.1\text{e}$ shifts the voltage dependence of activation to more negative voltages but does not affect current density in either of the two STAC3-HEK cell lines. (A–D) Current properties of $\text{Ca}_v1.1\text{a}$ (blue, $n = 15$) compared with $\text{Ca}_v1.1\text{e}$ (red, $n = 15$) in the HEK-STAC3 cell line. (E–H) Current properties of $\text{Ca}_v1.1\text{a}$ (blue, $n = 19$) compared with $\text{Ca}_v1.1\text{e}$ (red, $n = 15$) in the inducible cell line HEK-TetOn-STAC3 treated with DOX. (A and E) Exemplary current traces at V_{max} show similar activation kinetics of the $\text{Ca}_v1.1\text{a}$ and $\text{Ca}_v1.1\text{e}$ variants and no difference in the peak current density (I_{peak} ; peak current normalized to the cell size) in both the HEK-STAC3 (B) and HEK-TetOn-STAC3 (F) cell lines ($P = 0.94$ and $P = 0.56$, respectively). The current–voltage relationship (C and G) and the normalized steady-state activation curves (D and H) show that exclusion of exon 29 (in $\text{Ca}_v1.1\text{e}$) results in a 20.4- and 21.1-mV left shift of activation when expressed in the HEK-STAC3 and HEK-TetOn-STAC3 cell line, respectively. Mean \pm SEM; P values calculated with Student's t test (see Table 1 for parameters and statistics).

activation (Fig. 3, A–D; and Table 2). The activation kinetics were unaltered by coexpression of the γ_1 subunit (Fig. S1, A–D; and Table 2), in agreement with what had been observed in myotubes (Freise et al., 2000) but contrary to what was previously reported in tsA201 cells (Polster et al., 2016). More importantly, in contrast to $\text{Ca}_v1.1\text{a}$, coexpression of γ_1 had no effect on the current density of $\text{Ca}_v1.1\text{e}$ (Fig. 3, E–H; and Table 2), suggesting that the inclusion of the 19 amino acids encoded in exon 29 is essential for suppression of the $\text{Ca}_v1.1$ current by the γ_1 subunit.

The γ_1 subunit shifts the steady-state inactivation to more negative potentials in both $\text{Ca}_v1.1$ isoforms

The γ_1 subunit inhibits $\text{Ca}_v1.1$ currents not only by decreasing the current amplitude, but also by promoting inactivation. In fact, previous

studies demonstrated that, in the presence of γ_1 , the voltage dependence of inactivation shifted toward more negative potentials, while the voltage dependence of activation remained unaltered (Ahern et al., 2001; Freise et al., 2000; Held et al., 2002; Ursu et al., 2004).

To determine whether this γ_1 effect on $\text{Ca}_v1.1$ currents is also restricted to the adult $\text{Ca}_v1.1\text{a}$ isoform, we performed a steady-state inactivation protocol comparing the current size of test pulses before and after 45-s conditioning prepulses at incrementally increasing potentials (Fig. 4 A, inset). The normalized steady-state inactivation was plotted as a function of the prepulse potential. As previously demonstrated, coexpression of the γ_1 subunit resulted in a robust left shift in the voltage dependence of inactivation of the adult $\text{Ca}_v1.1\text{a}$ isoform (Fig. 4 A). In the presence of γ_1 , the half-maximal inactivation potential was

Table 1. Current activation properties of $\text{Ca}_v1.1\text{a}$ and $\text{Ca}_v1.1\text{e}$ expressed in HEK-STAC3 and HEK-TetOn-STAC3 cells

Property	HEK-STAC3			HEK-TetOn-STAC3		
	$\text{Ca}_v1.1\text{a}$	$\text{Ca}_v1.1\text{e}$	P value (t test)	$\text{Ca}_v1.1\text{a}$	$\text{Ca}_v1.1\text{e}$	P value (t test)
I_{peak} (pA/pF)	-19.8 ± 2.7	-19.5 ± 2.4	0.94	-18.2 ± 3.1	-21.3 ± 4.5	0.56
$V_{1/2}$ activation (mV)	24.4 ± 0.7	4.0 ± 1.0	****	24.1 ± 1.4	3.0 ± 1.5	****
k activation (mV)	8.1 ± 0.4	7.1 ± 0.2	0.03*	7.0 ± 0.5	5.3 ± 0.3	0.011*
V_{rev} (mV)	86.3 ± 1.2	75.3 ± 1.1	****	81.2 ± 1.7	72.8 ± 1.6	0.0013**
Time to peak (ms)	173.1 ± 10.8	162.6 ± 12.0	0.52	198.3 ± 20.4	184.1 ± 14.3	0.59
n	15	15		19	15	

Data are expressed as mean values \pm SEM. Statistically significant: *, $P < 0.05$; **, $P < 0.01$; ***, $P < 0.001$; ****, $P < 0.0001$.

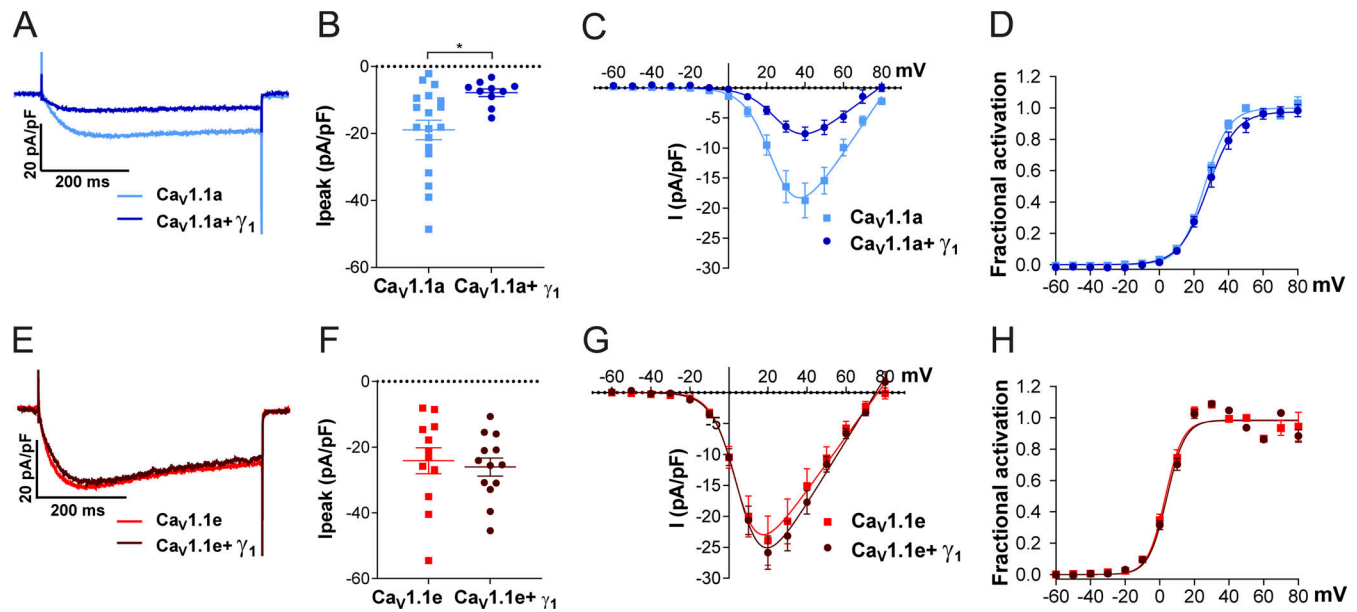


Figure 3. **Coexpression of γ_1 reduces the current density in $\text{Ca}_v1.1a$ but not in $\text{Ca}_v1.1e$.** (A–D) Current properties of the adult splice variant $\text{Ca}_v1.1a$ (blue, $n = 19$) compared with $\text{Ca}_v1.1a$ coexpressed with γ_1 ($\text{Ca}_v1.1a + \gamma_1$, dark blue, $n = 10$). (E–H) Current properties of the embryonic splice variant $\text{Ca}_v1.1e$ (red, $n = 12$) compared with $\text{Ca}_v1.1e + \gamma_1$ (dark red, $n = 13$). (A–H) Exemplary current traces at V_{\max} (A) and the scatter plot of the peak current density (I_{peak} ; B) show a significant reduction ($P = 0.012$) when coexpressing γ_1 with $\text{Ca}_v1.1a$. In contrast, when coexpressing γ_1 with $\text{Ca}_v1.1e$ (E and F), no difference in current density was observed ($P = 0.69$). The current–voltage relationship (C and G) and the fractional steady-state activation curves (D and H) show no effect of γ_1 on the voltage dependence of activation when coexpressed with $\text{Ca}_v1.1a$ or $\text{Ca}_v1.1e$. Mean \pm SEM; P values calculated with Student's t test. *, $P < 0.05$ (for parameters and statistics, see Table 2).

shifted by 14.1 mV toward more hyperpolarizing potentials (Fig. 4 B and Table 2).

Surprisingly, these effects were recapitulated with the embryonic $\text{Ca}_v1.1e$ isoform. In the presence of the γ_1 subunit, the

half-maximal inactivation potential was shifted to hyperpolarizing potentials by 13.7 mV (Fig. 4, C and D; and Table 2). These results suggest that, although the γ_1 subunit fails to suppress the current of the embryonic $\text{Ca}_v1.1e$ splice variant by

Table 2. **Current properties (activation and inactivation) of $\text{Ca}_v1.1a$ and $\text{Ca}_v1.1e$ in the presence and absence of γ_1**

Property	$\text{Ca}_v1.1a$	$\text{Ca}_v1.1a + \gamma_1$	P value	$\text{Ca}_v1.1e$	$\text{Ca}_v1.1e + \gamma_1$	P value
I_{peak} (pA/pF)	-18.9 ± 2.9	-7.8 ± 1.2	0.012*	-24.1 ± 4.0	-26.1 ± 2.7	0.69
$V_{1/2}$ activation (mV)	26.3 ± 1.0	29.4 ± 2.0	0.14	3.9 ± 1.1	4.5 ± 0.9	0.68
k activation (mV)	6.8 ± 0.2	8.3 ± 0.8	0.03*	5.1 ± 0.3	5.2 ± 0.2	0.70
V_{rev} (mV)	83.4 ± 1.1	78.6 ± 2.8	0.07	75.7 ± 2.0	76.0 ± 1.3	0.90
Time to peak (ms)	150.1 ± 18.0	102.9 ± 15.0	0.08	104.4 ± 11.0	97.1 ± 13.3	0.67
τ_{mono} activation (ms)	35.1 ± 3.0	32.9 ± 2.9	0.65	30.3 ± 5.5	23.7 ± 4.0	0.19
τ_{slow} activation (ms)				107.4 ± 39.9	79.6 ± 21.2	0.53
A_{slow} activation (%)				18.7 ± 6.9	31.0 ± 11.8	0.41
τ_{fast} activation (ms)				26.4 ± 6.1	17.1 ± 4.4	0.23
A_{fast} activation (%)				81.3 ± 6.9	69.0 ± 11.8	0.41
n (activation)	19	10		12	13	
$V_{1/2}$ inactivation (mV)	-16.9 ± 2.6	-31.0 ± 5.3	0.04*	-28.6 ± 1.7	-42.3 ± 1.9	***
I_{residual} (%)	18.7 ± 7.4	14.7 ± 4.6	0.66	9.8 ± 3.1	3.9 ± 1.3	0.13
k inactivation (mV)	8.1 ± 0.4	7.9 ± 0.9	0.89	7.0 ± 0.9	7.3 ± 0.3	0.79
τ_{mono} inactivation (ms)	$2,062.4 \pm 525.5$	$1,389.5 \pm 251.5$	0.32	$2,159.8 \pm 278.5$	$1,453.2 \pm 230.3$	0.15
n (inactivation)	6	6		7	6	

Data are expressed as mean values \pm SEM. Statistically significant: *, $P < 0.05$; ***, $P < 0.001$.

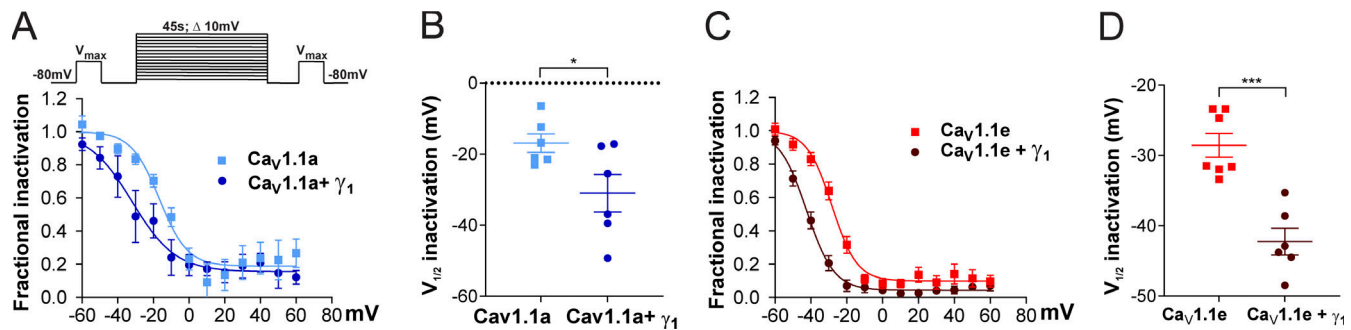


Figure 4. γ_1 Left shifts the steady-state inactivation of both $\text{Ca}_v1.1a$ and $\text{Ca}_v1.1e$ currents. (A–D) Steady-state inactivation of $\text{Ca}_v1.1a$ (A and B) and $\text{Ca}_v1.1e$ (C and D) currents in the presence or in the absence of γ_1 . The inset in A shows the steady-state inactivation protocol. Fractional inactivation curves and scatter plot of $V_{1/2}$ of $\text{Ca}_v1.1a$ currents (blue, $n = 6$) compared with $\text{Ca}_v1.1a + \gamma_1$ currents (dark blue, $n = 6$; A and B); the same for $\text{Ca}_v1.1e$ (red, $n = 7$) and $\text{Ca}_v1.1e + \gamma_1$ currents (dark red, $n = 6$; C and D). The voltage dependence of inactivation is left shifted in $\text{Ca}_v1.1a + \gamma_1$ (14.1 mV, $P = 0.04$) and $\text{Ca}_v1.1e + \gamma_1$ (13.7 mV, $P < 0.001$). Mean \pm SEM; P values calculated with Student's t test. *, $P < 0.05$; ***, $P < 0.001$.

reducing its amplitude (Fig. 3, E–G), it still inhibits $\text{Ca}_v1.1e$ currents by left-shifting the steady-state inactivation.

The γ_1 subunit was also reported to accelerate the inactivation kinetics of $\text{Ca}_v1.1$ (Ahern et al., 2001; Freise et al., 2000). Accordingly, the time constant of inactivation was reduced to 67% in the presence of γ_1 for both $\text{Ca}_v1.1a$ and $\text{Ca}_v1.1e$, although not to a statistically significant extent (Fig. S1, E–H; and Table 2).

The γ_1 subunit increases membrane expression of both $\text{Ca}_v1.1$ isoforms

$\text{Ca}_v1.1$ is the only 1 out of the 10 voltage-gated calcium channels that expresses poorly in non-muscle cells, unless the adaptor protein STAC3 is coexpressed (Polster et al., 2015). Recently it was shown that the γ_1 subunit also supports robust membrane expression of $\text{Ca}_v1.1a$ in tsA201 cells; although in the absence of STAC3, these channels produce only very small calcium currents (Polster et al., 2016). To examine whether the γ_1 subunit supports only the membrane targeting of the adult $\text{Ca}_v1.1a$ isoform or also of the embryonic $\text{Ca}_v1.1e$, we established a dual-labeling approach, originally developed by the lab of Henry Colecraft (Fang and Colecraft, 2011; Yang et al., 2010), to identify and quantify membrane-inserted $\text{Ca}_v1.1$ channels. To this end, a 13 amino acid high-affinity BBS was introduced into the extracellular IIS5–IIS6 domain of GFP- $\text{Ca}_v1.1a$ and GFP- $\text{Ca}_v1.1e$. Then, the channels expressed on the cell surface of HEK cells (expressing β_3 and $\alpha_2\delta-1$) were labeled by exposing unpermeabilized living cells to biotinylated BTX and subsequently to streptavidin-coated quantum dots (QD₆₅₅; Fig. 5 A). Hence, the GFP fluorescence of a cell measures the total $\text{Ca}_v1.1$ expression, and the QD₆₅₅ fluorescence quantifies the fraction of surface-expressed $\text{Ca}_v1.1$ channels.

In cells expressing $\text{Ca}_v1.1a$ alone, we detected minimal QD₆₅₅ fluorescence in the plasma membrane. By contrast, coexpression of STAC3 or γ_1 , individually or together, resulted in robust $\text{Ca}_v1.1a$ membrane targeting (Fig. 5 B). To quantify membrane-inserted $\text{Ca}_v1.1$ channels, we used flow cytometry analysis, which measures the fluorescence signals of a multitude of individual cells (Fig. 5 D). This analysis confirmed the lack of a robust QD₆₅₅ fluorescence signal in cells expressing only GFP- $\text{Ca}_v1.1a$ but the presence of a strong QD₆₅₅ fluorescence in cells

coexpressing GFP- $\text{Ca}_v1.1a$ together with STAC3, γ_1 , or both. In four independent experiments, cells coexpressing STAC3 on average displayed a 140% increase of surface-expressed $\text{Ca}_v1.1a$, cells coexpressing γ_1 displayed an 80% increase, and cells expressing both STAC3 and γ_1 subunits displayed a 180% increase compared with cells expressing $\text{Ca}_v1.1a$ alone (Fig. 5 F). These results corroborate the importance of STAC3 and γ_1 for $\text{Ca}_v1.1a$ plasma membrane expression (Niu et al., 2018; Polster et al., 2016; Polster et al., 2015).

We then analyzed the effect of the STAC3 and γ_1 subunits on membrane expression of the embryonic $\text{Ca}_v1.1e$ isoform. In contrast to the adult isoform, the embryonic $\text{Ca}_v1.1e$ channel showed substantial membrane staining even when expressed alone (Fig. 5, C [top] and E [left]). Nevertheless, coexpression of STAC3 and γ_1 , individually or together, further increased the amount of QD₆₅₅ fluorescence (Fig. 5, C and E). In four independent experiments, cells coexpressing STAC3 displayed a 70% increase of surface-expressed $\text{Ca}_v1.1e$, cells coexpressing γ_1 displayed a 50% increase, and the ones expressing both STAC3 and γ_1 subunits displayed an 80% increase compared with cells expressing $\text{Ca}_v1.1e$ alone (Fig. 5 G).

Altogether, these results demonstrate that, although the γ_1 subunit fails to modulate the current amplitude of the embryonic $\text{Ca}_v1.1e$ isoform, it still modulates its steady-state inactivation and surface trafficking. Moreover, the reduction of current density induced by γ_1 cannot be explained by reduced channel availability at the cell surface.

$\text{Ca}_v1.1$ – γ_1 ion-pair partners predicted by structure modeling are not essential for $\text{Ca}_v1.1a$ -specific current reduction by γ_1

Because the recent cryo-EM structure of $\text{Ca}_v1.1$ revealed that the γ_1 subunit interacts with IVS3–S4 (Wu et al., 2016; Wu et al., 2015), and because we found that γ_1 fails to inhibit the current amplitude of the embryonic $\text{Ca}_v1.1e$ isoform (Fig. 2 E), which lacks 19 amino acids in the IVS3–S4 linker, we hypothesized that γ_1 and the IVS3–S4 linker of $\text{Ca}_v1.1a$ may establish an interaction responsible for the current inhibition in $\text{Ca}_v1.1a$. To identify putative interaction partners between the IVS3–S4 linker and γ_1 , we generated a structural model of the $\text{Ca}_v1.1$ channel based on the published cryo-EM structure (Wu et al., 2016; Fig. 6). We

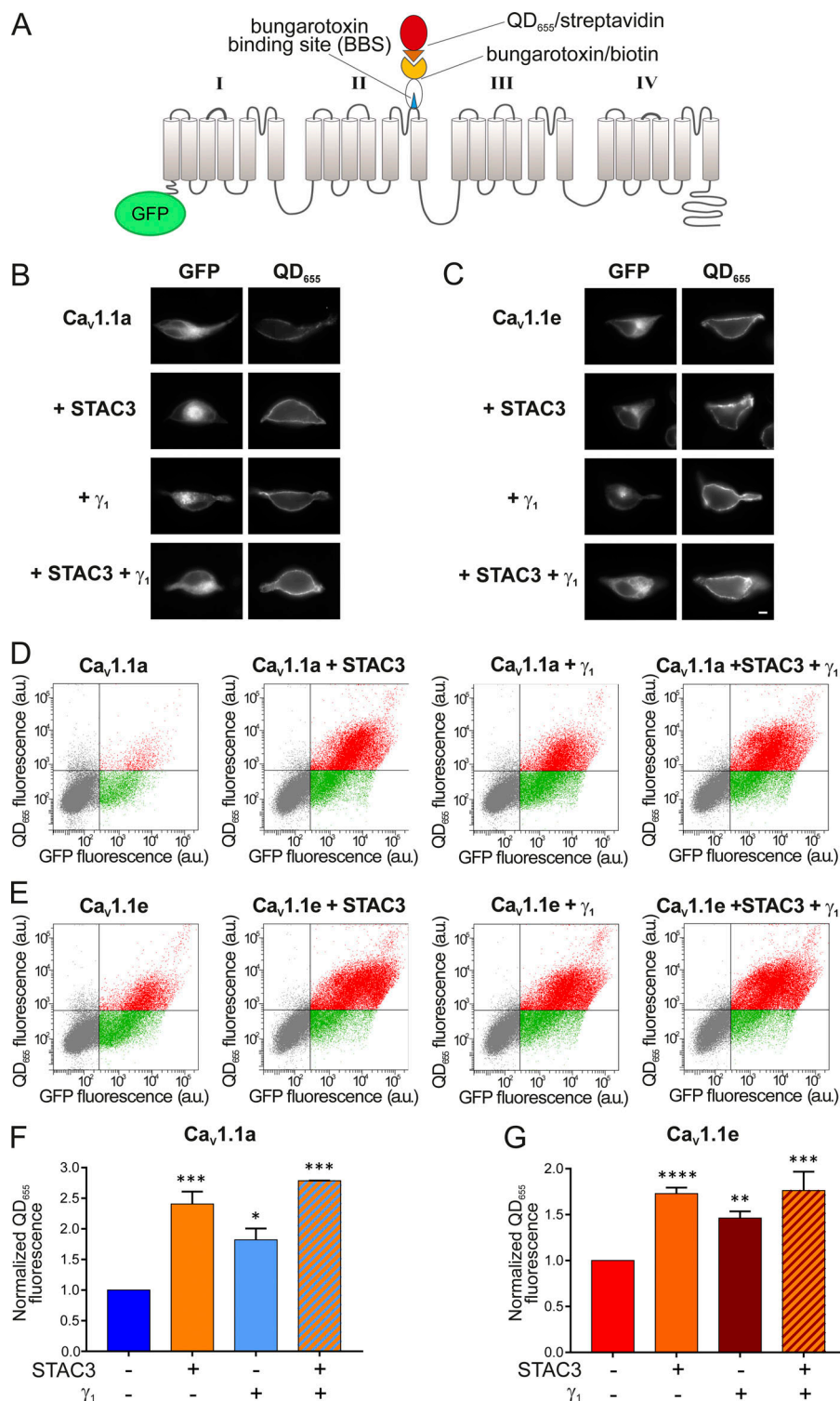


Figure 5. γ_1 increases the surface density of both $\text{Ca}_v1.1a$ and $\text{Ca}_v1.1e$ isoforms. (A) Scheme displaying the strategy to detect $\text{Ca}_v1.1$ channels expressed on the plasma membrane of HEK cells (stably expressing β_3 and $\alpha_2\delta-1$). The introduction of the 13 amino acid BBS in the extracellular domain of GFP- $\text{Ca}_v1.1a$ or GFP- $\text{Ca}_v1.1e$ allowed the selective labeling of channels in the membrane by sequentially incubating the unpermeabilized cells with biotinylated BTX and streptavidin-conjugated quantum dots (QD₆₅₅). (B) From top to bottom, representative images of HEK cells expressing the adult GFP- $\text{Ca}_v1.1a$ isoform alone, with STAC3, with γ_1 , and with both STAC3 and γ_1 . (C) The same for HEK cells expressing the embryonic GFP- $\text{Ca}_v1.1e$ isoform. Scale bar, 2 μm . (D and E) Representative raw data from flow cytometry experiments showing the GFP and the QD₆₅₅ signal for cells expressing GFP- $\text{Ca}_v1.1a$ (D) or GFP- $\text{Ca}_v1.1e$ (E) alone, with STAC3, with γ_1 , and with both STAC3 and γ_1 . The vertical and horizontal lines represent threshold values determined using untransfected cells, and cells exposed only to QD₆₅₅. Single cells are depicted as dots, which have been colored in gray (untransfected), green (transfected, lacking surface expression), or red (transfected with appreciable surface expression). (F and G) Normalized mean QD₆₅₅ fluorescence signals across separate flow cytometry experiments ($n = 4$). Data were normalized to the QD₆₅₅ signals of cells expressing only GFP- $\text{Ca}_v1.1$. In F, the conditions with STAC3 (***, $P = 0.0003$), γ_1 (*, $P = 0.0143$), and STAC3 + γ_1 (***, $P = 0.0002$) are significantly different from the control GFP- $\text{Ca}_v1.1a$ using one-way ANOVA and Tukey post-hoc mean comparison. In G, the conditions with STAC3 (****, $P < 0.0001$), γ_1 (**, $P = 0.0019$), and STAC3 + γ_1 (***, $P = 0.0002$) are significantly different from the control GFP- $\text{Ca}_v1.1e$ using one-way ANOVA and Tukey post hoc mean comparison.

used Rosetta computational modeling software (Bender et al., 2016; Rohl et al., 2004) to model the structure of the IVS3-S4 linker of $\text{Ca}_v1.1a$. The resulting structure predicts a putative interaction of residues D1223 and D1225 of the IVS3-S4 linker of $\text{Ca}_v1.1a$ with residue R160 in the second extracellular loop of the γ_1 subunit (Figs. 7 A and 6 B). To test whether the observed inhibition of the $\text{Ca}_v1.1a$ current amplitude by γ_1 is dependent on this ionic interaction, we performed site-directed mutagenesis

to substitute the involved residues with alanines, which deletes all interactions made by side-chain atoms beyond the β carbon (Wells, 1991). However, mutation of residue R160 of the γ_1 subunit to an alanine did not diminish its ability to inhibit the current amplitude of $\text{Ca}_v1.1a$ (Fig. 7, A–D; and Table 3). Also, simultaneously mutating both D1223 and D1225 of $\text{Ca}_v1.1a$ did not alter the ability of γ_1 to reduce the current amplitude of $\text{Ca}_v1.1a$ (Fig. 7, E–H; and Table 3). Together, these results indicate

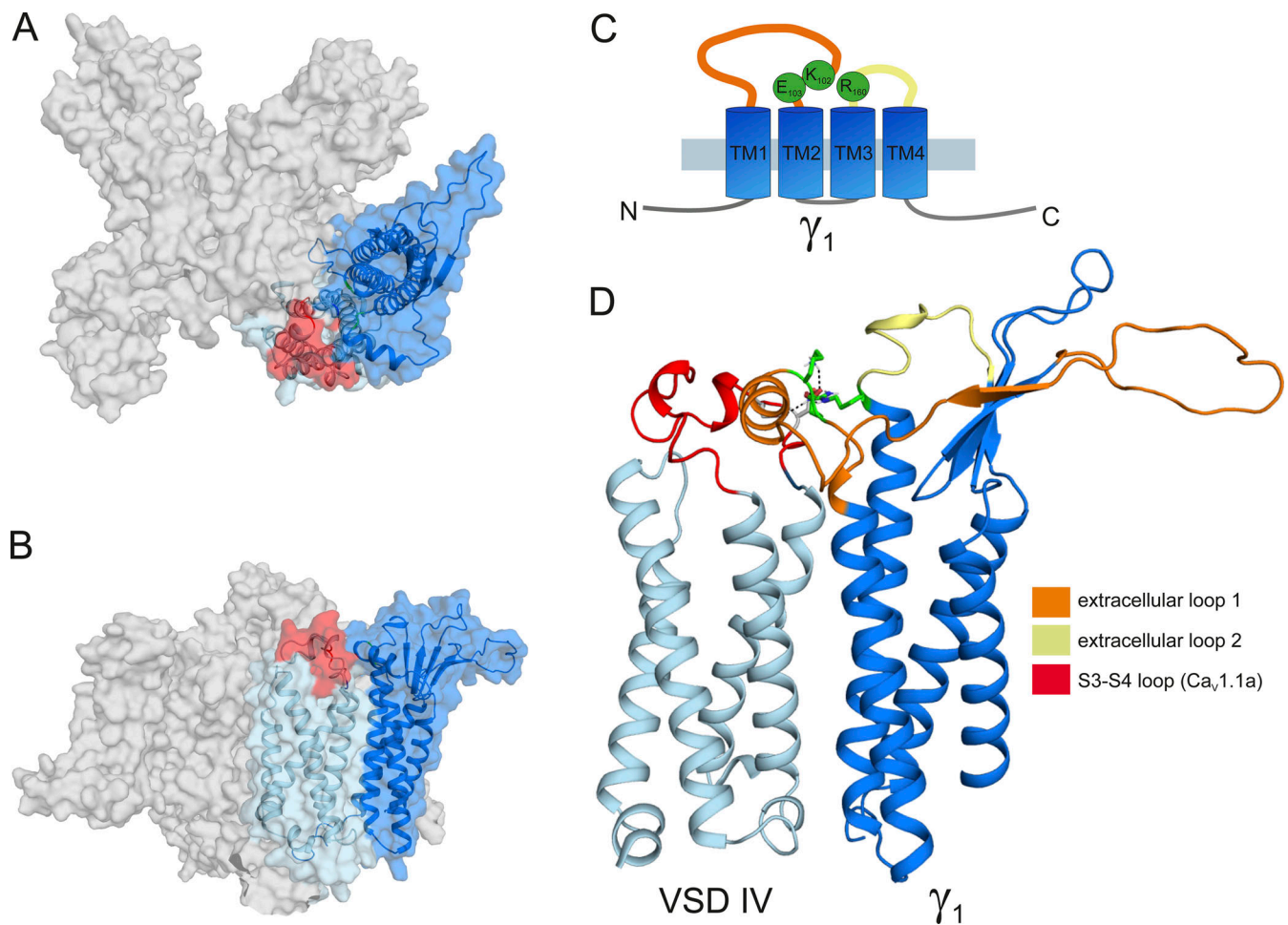


Figure 6. Structure modeling of Ca_v1.1a in complex with the γ_1 subunit. (A) Top view of the structure model of the human Ca_v1.1 α_1 subunit in complex with the γ_1 subunit refined with molecular dynamics simulation in a membrane environment based on the 3.6-Å structure of rabbit Ca_v1.1 (Wu et al., 2016). VSD IV (light blue) is interacting with the γ_1 subunit (marine). The alternatively spliced exon 29 (red) is inserted in the IVS3-S4 linker of Ca_v1.1a. (B) Side view of the structure model of Ca_v1.1 with the γ_1 subunit. (C) Cartoon showing the domain organization of γ_1 , with the mutated residues R160, K102, and E103 in green. (D) Close-up of the interaction site of the VSD IVS3-S4 loop with the γ_1 subunit, highlighting the extracellular loops of the γ_1 subunit. The extracellular loop 1 of γ_1 is in the same orientation as presented in Fig. 7, A, E, and M, and residue R160 is highlighted in green.

that this putative interaction between the IVS3-S4 linker of Ca_v1.1a and the γ_1 subunit is dispensable for current amplitude inhibition by γ_1 .

Previously, it has been suggested that the N-terminal half of the γ_1 subunit, including the first two transmembrane domains, mediates its interaction with the calcium channel and is responsible for suppressing the current amplitude of Ca_v1.1 (Arikkath et al., 2003). Because the analyzed R160A mutation is located outside of this region in the C-terminal half of the γ_1 subunit protein, we further modeled the structure of the extensive extracellular loop located in the first half of the γ_1 subunit and searched it for possible interaction sites with the IVS3-S4 linker of Ca_v1.1a. We identified putative ionic interactions of residues D1225 and R1229 in the IVS3-S4 linker of Ca_v1.1a with K102 and E103 positioned in the first extracellular domain of the γ_1 subunit (Fig. 7 I, Table 3, and Fig. 6). However, mutation of K102 and E103 to alanines did not alter the ability of γ_1 to inhibit the calcium channel current amplitude (Fig. 7, J-L; and Table 3). Finally, to exclude the possibility that the interaction between

the IVS3-S4 linker of Ca_v1.1a with either one of the two extracellular loops of γ_1 was sufficient to suppress the calcium channel current amplitude, we combined the R160A and K102A/E103A mutations (Fig. 7 M). However, this triple-mutant γ_1 was also capable of inhibiting the current amplitude of Ca_v1.1a to levels similar to the wild type γ_1 (Fig. 7, N-P; and Table 3). Together, these mutagenesis experiments suggest that the current-inhibiting effect of γ_1 is not mediated by the direct ionic interactions between γ_1 and the IVS3-S4 loop of Ca_v1.1a, at least not those predicted by our structure modeling.

Discussion

Whereas the role of the auxiliary $\alpha_2\delta$ and β subunits in subcellular targeting and gating modulation have been extensively studied for high voltage activated calcium channels in heterologous cells, this has not been the case for the γ_1 subunit. γ_1 is a specific subunit of the skeletal muscle Ca_v1.1 isoform and, until recently, Ca_v1.1 had resisted efficient functional expression in

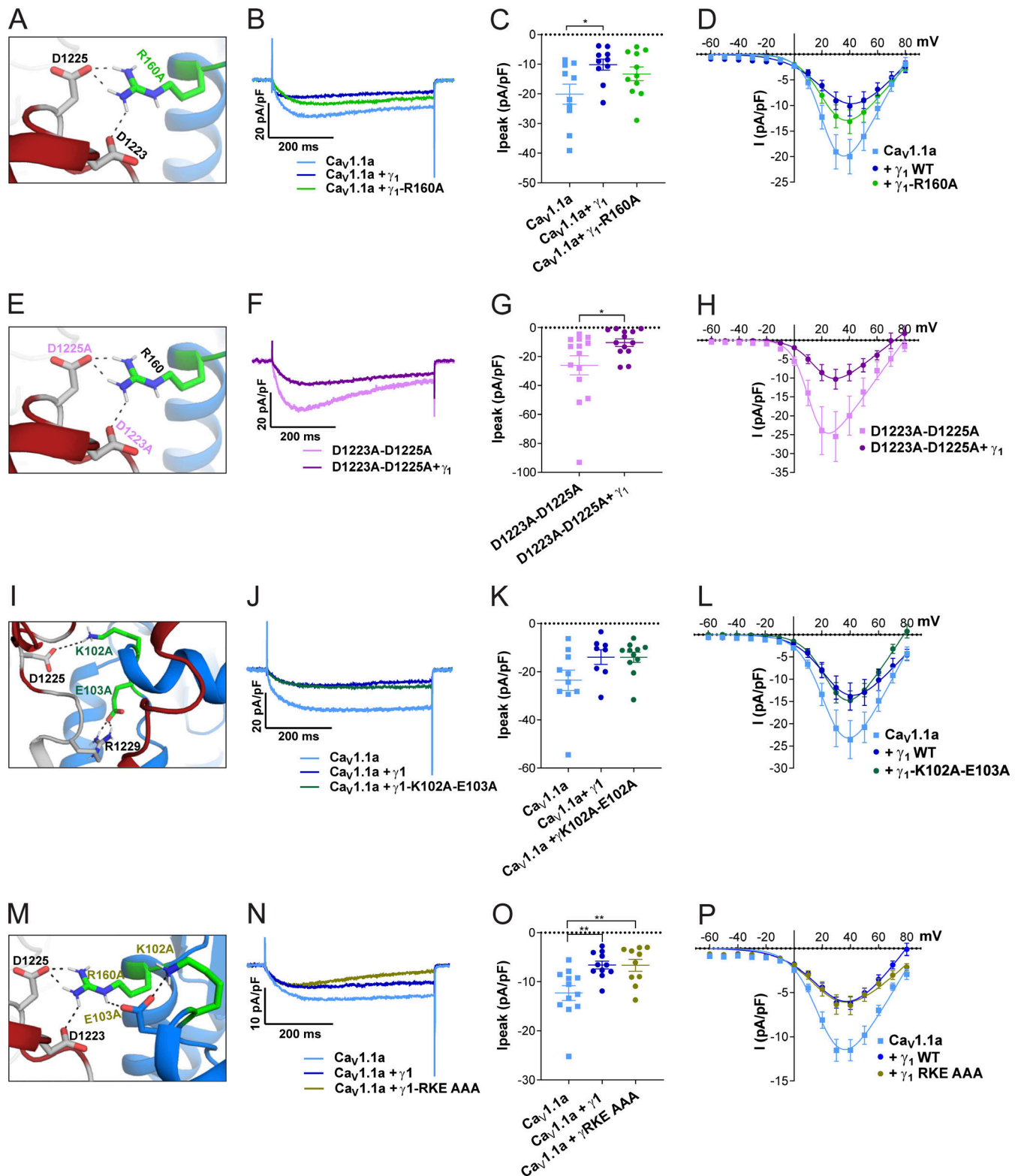


Figure 7. The putative interactions between the IVS3-S4 loop and γ_1 identified by structure modeling are dispensable for $\text{Ca}_v1.1a$ current reduction. (A–H) Structure modeling of $\text{Ca}_v1.1a$ and γ_1 indicates interactions of R160 (γ_1) with D1223 and D1225 ($\text{Ca}_v1.1a$). Neutralizing the putative $\text{Ca}_v1.1a$ interaction partner (R160A; A) or the γ_1 interaction partners (D1223A and D1225A; E), did not impair current reduction by γ_1 (B–D and F–H). (I–L) Structure modeling of $\text{Ca}_v1.1a$ and γ_1 indicates further interactions of K102 and E103 (γ_1) with D1225 and R1229 ($\text{Ca}_v1.1a$). Neutralizing both of these putative $\text{Ca}_v1.1a$ interaction partners to alanine (K102A/E103A; I) did not abolish the ability of γ_1 to reduce $\text{Ca}_v1.1a$ current (J and K). (M–P) Concomitant mutation of all three γ_1 residues involved in these putative interactions did not abolish the current reduction by γ_1 (N–P). Exemplary current traces at V_{max} (B, F, J, and N); scatter plots of I_{peak} (C, G, K, and O); and current–voltage relationship (D, H, L, and P). Mean \pm SEM; P values calculated with ANOVA and Tukey's post-hoc test. *, $P < 0.05$; **, $P < 0.01$.

Table 3. Current activation properties of Ca_v1.1a-D1223A-D1225A, γ_1 -R160A, γ_1 -K102A-E103A, and γ_1 -R160A-K102A-E103A (RKE AAA) mutants

Property	Ca _v 1.1a	Ca _v 1.1a + γ_1	P value (ANOVA)	Ca _v 1.1a + γ_1 -R160	P value (ANOVA)
I_{peak} (pA/pF)	-20.1 ± 3.4	-10.1 ± 1.9	0.04*	-13.3 ± 2.3	0.20
$V_{1/2}$ activation (mV)	23.1 ± 0.6	30.7 ± 2.2	0.004**	24.1 ± 1.3	0.88
k activation (mV)	7.0 ± 0.3	13.1 ± 1.8	0.001**	8.5 ± 0.4	0.58
V_{rev} (mV)	82.7 ± 2.2	86.1 ± 3.9	0.65	87.4 ± 1.3	0.42
Time to peak (ms)	131.8 ± 18.8	102.6 ± 8.4	0.26	95.3 ± 8.9	0.12
n	10	10		11	
	Ca _v 1.1a D1223A–1225A	Ca _v 1.1a D1223A–1225A + γ_1	P value (t test)		
I_{peak} (pA/pF)	-26.1 ± 6.6	-10.4 ± 2.6	0.04*		
$V_{1/2}$ activation (mV)	12.8 ± 0.8	15.8 ± 0.9	0.02*		
k activation (mV)	6.3 ± 0.4	7.1 ± 0.5	0.22		
V_{rev} (mV)	73.5 ± 2.5	69.7 ± 4.3	0.44		
Time to peak (ms)	87.2 ± 11.0	66.6 ± 10.7	0.20		
n	14	13			
	Ca _v 1.1a	Ca _v 1.1a + γ_1	P value (ANOVA)	Ca _v 1.1a + γ_1 -K103A-E104A	P value (ANOVA)
I_{peak} (pA/pF)	-23.6 ± 4.2	-13.9 ± 3.1	0.13	-14.0 ± 2.1	0.09
$V_{1/2}$ activation (mV)	25.1 ± 1.0	26.9 ± 0.9	0.40	28.2 ± 0.9	0.06
k activation (mV)	8.7 ± 0.5	9.8 ± 0.5	0.20	8.7 ± 0.4	0.99
V_{rev} (mV)	86.7 ± 1.8	91.8 ± 2.0	0.24	81.2 ± 2.7	0.17
Time to peak (ms)	121.5 ± 18.5	99.8 ± 23.1	0.69	108.5 ± 13.3	0.85
n	10	8	–	11	
	Ca _v 1.1a	Ca _v 1.1a + γ_1	P value (ANOVA)	Ca _v 1.1a + γ_1 -RKE AAA	P value (ANOVA)
I_{peak} (pA/pF)	-12.3 ± 1.5	-6.6 ± 0.8	0.006**	-6.6 ± 1.2	0.008**
$V_{1/2}$ activation (mV)	20.6 ± 0.9	28.2 ± 3.3	0.13	25.7 ± 4.2	0.38
k activation (mV)	8.9 ± 0.6	13.9 ± 2.2	0.07	13.4 ± 2.0	0.12
V_{rev} (mV)	89.8 ± 2.0	83.2 ± 4.2	0.24	92.5 ± 2.9	0.76
Time to peak (ms)					
n	12	11		10	

Data are expressed as mean values ± SEM. Statistically significant: *, $P < 0.05$; **, $P < 0.01$.

heterologous expression systems. Only since the discovery of STAC3 as an essential component of the Ca_v1.1 channel complex, permitting the reliable heterologous expression of Ca_v1.1, have such analyses been possible (Horstick et al., 2013; Nelson et al., 2013; Polster et al., 2015). Here, we developed and validated two HEK cell lines stably expressing STAC3 (plus $\alpha_2\delta$ -1 and β_3), which proved to be a convenient and efficient heterologous expression system for Ca_v1.1. By coexpression of Ca_v1.1 and γ_1 in these cells, we found three effects of the γ_1 subunit: facilitated membrane expression of Ca_v1.1, a reduction of the current density, and a shift of steady-state inactivation to hyperpolarizing potentials. The effects of the γ_1 subunit on the two splice variants of Ca_v1.1 expressed in our new STAC3-HEK cell lines revealed a novel, isoform-dependent mechanism of channel modulation by this subunit. Although γ_1 equally supports membrane expression of Ca_v1.1a and Ca_v1.1e, it functions only as a negative regulator of the adult Ca_v1.1a splice variant. This differential regulation of current density is mediated by

the inclusion of the alternatively spliced exon 29 in the extracellular loop connecting helices S3 and S4 in repeat IV, but it does not require the direct ionic interactions between this loop and the γ_1 subunit. Another novel finding is that in both the adult and embryonic Ca_v1.1 splice variants, γ_1 reduces steady-state inward current at more negative voltages by shifting the voltage dependence of steady-state inactivation, but not of activation, to more negative voltages and by promoting the time course of current inactivation.

The γ_1 subunit supports membrane expression of Ca_v1.1

The substantially increased surface expression induced by coexpression of γ_1 observed with extracellular BTX labeling and flow cytometry did not translate into increased current densities. This is consistent with the observation that in γ_1 -null mouse muscle, in which STAC3 is endogenously expressed, the expression levels of Ca_v1.1 are similar to those of wild type mice (Arikath et al., 2003). In our experiments, this is explained by

the observation that the effects of γ_1 and STAC3 on membrane expression are not additive, and therefore γ_1 does not significantly increase $\text{Ca}_v1.1$ beyond the level already achieved by STAC3. Apparently, an independent component must be limiting for membrane targeting. The effect of γ_1 on membrane targeting in heterologous cells is consistent with a previous immunocytochemistry and charge movement analysis showing that in the absence of STAC3, the γ_1 subunit supports robust membrane expression of $\text{Ca}_v1.1$ in tsA201 cells, while sustaining only very small currents (Polster et al., 2016). In contrast, an earlier Western blot analysis of tsA201 cells lysates reported that coexpression of γ_1 reduces the levels of $\text{Ca}_v1.1$ protein expression (Sandoval et al., 2007). In sum, our results corroborate the findings that the γ_1 subunit supports membrane expression of $\text{Ca}_v1.1$ in heterologous cell systems in a splice variant-independent manner, possibly by masking retention motifs on the C-terminus (Niu et al., 2018), but without adding to the calcium influx.

The γ_1 subunit promotes steady-state inactivation in $\text{Ca}_v1.1a$ and $\text{Ca}_v1.1e$

Functionally, the two negative actions of γ_1 on $\text{Ca}_v1.1$ currents dominate. The observed decrease in current amplitude and left-shift of steady-state inactivation are in general agreement with previous studies in muscle cells (Ahern et al., 2001; Freise et al., 2000) as well as in tsA201 cells expressing $\text{Ca}_v1.1a$ (Polster et al., 2016). Limiting calcium influx through $\text{Ca}_v1.1$ during muscle activity is tolerable because of the principal role of $\text{Ca}_v1.1$ as a voltage sensor in skeletal muscle EC coupling (Schneider and Chandler, 1973; Rios and Brum, 1987). At the same time, it is important to limit interference of calcium influx with other calcium signaling events, such as those regulating fiber type specification, and to avoid adverse effects of calcium overload on mitochondrial integrity (Sultana et al., 2016). Previously, we pointed out how intrinsic mechanisms in the $\text{Ca}_v1.1$ α_{1S} subunit and the actions of auxiliary subunits cooperate in limiting the calcium currents in skeletal muscle (Tuluc et al., 2009; Flucher et al., 2005). Whereas the $\alpha_2\delta-1$ subunit slows down the activation, the γ_1 subunit promotes voltage-dependent inactivation at more negative voltages. This effect was equally observed in the adult and, as shown here for the first time, the embryonic splice variant. Together with the observed increase in membrane targeting, this is the first experimental evidence demonstrating that the γ_1 subunit functionally interacts with the embryonic splice variant $\text{Ca}_v1.1e$. Therefore, this modulatory effect is independent of the length of the extracellular loop connecting helices IVS3 and IVS4.

The γ_1 subunit reduces the current amplitude specifically in $\text{Ca}_v1.1a$

The most interesting finding of this study is the differential down-regulation of calcium currents in $\text{Ca}_v1.1a$ versus $\text{Ca}_v1.1e$. The small current size is one of the hallmarks of skeletal muscle calcium currents. Our results demonstrate that the γ_1 subunit is a major determinant of this reduced current density. Whereas in skeletal muscle the adult and embryonic $\text{Ca}_v1.1$ splice variants differ substantially in voltage dependence of current activation

and in current size, the currents recorded in the HEK cells (stably expressing $\alpha_2\delta-1$, β_3 , and STAC3) reproduced the difference in $V_{1/2}$ of activation, but not in current density. Apparently, this difference is due to the lack of one or more muscle-specific factors in the heterologous expression system. As coexpression of γ_1 restored the reduced current density in $\text{Ca}_v1.1a$ compared with $\text{Ca}_v1.1e$, the γ_1 subunit is such a factor. Quantitatively, the difference in current density between the two splice variants was still smaller than that observed when the same constructs were expressed in dysgenic myotubes (Tuluc et al., 2016; Tuluc et al., 2009). Therefore, it is likely that other modulatory mechanisms present in the native environment of the channel in the skeletal muscle triads contribute to the full expression of this splice variant-specific difference. The γ_1 subunit is one of two proteins shown to differentially modulate the current properties of the two $\text{Ca}_v1.1$ splice variants, along with RYR1 (Benedetti et al., 2015), demonstrating the importance of the native cellular environment for the accurate expression of physiological current properties. Notably, γ_1 does not reduce the current density of $\text{Ca}_v1.1a$ by decreasing its plasma membrane expression. As previously shown, $\text{Ca}_v1.1e$ has a higher open probability than $\text{Ca}_v1.1a$ in skeletal myotubes (Tuluc et al., 2009). Therefore, the most likely explanation is that γ_1 decreases the channel's maximal open probability in a splice variant-specific manner.

The sole difference in the primary structure between the embryonic and adult splice variants is the inclusion of 19 amino acids coded in exon 29 in the IVS3-S4 loop of $\text{Ca}_v1.1a$. Apparently, this difference determines the action of the γ_1 subunit on current size. There are two possible mechanisms how inclusion of exon 29 can enable this functional interaction with γ_1 : direct interactions between the IVS3-S4 loop and γ_1 or the stabilization of a conformation of the channel complex by inclusion of exon 29 that renders $\text{Ca}_v1.1a$ susceptible to this particular γ_1 modulation. As the first possibility is amenable to experimental testing, we examined it by identifying and mutating putative interaction sites on both channel subunits. However, none of these ion pairs seemed to be essential for the current-reducing action of γ_1 . This result is in agreement with previous findings showing that $\text{Ca}_v1.1$ current reduction is mediated by the first two transmembrane domains of γ_1 , and that the extracellular loop is dispensable for this interaction (Arikkath et al., 2003). Therefore, it is unlikely that this effect is mediated by the direct interaction of the γ_1 subunit with the IVS3-S4 loop, although our experiments do not entirely rule out this possibility.

Given that the $\text{Ca}_v1.1$ structure identified the II and III transmembrane domains of γ_1 as the ones involved in the interaction with the IVS3-S4 of $\text{Ca}_v1.1$ (Wu et al., 2016), and that the first two transmembrane domains of γ_1 were sufficient for reconstituting the current reduction (Arikkath et al., 2003), we can deduce that an interaction between the second transmembrane domain of γ_1 and the IVS4 of $\text{Ca}_v1.1$ is the most likely scenario for mediating the current-reducing effect. We therefore conclude that insertion of exon 29 into the IVS3-S4 loop alters the conformation of the channel in a way that enables it to respond to the inclusion of γ_1 with a reduced current density (Fig. 8 A). Notably, the left-shifted activation in $\text{Ca}_v1.1e$

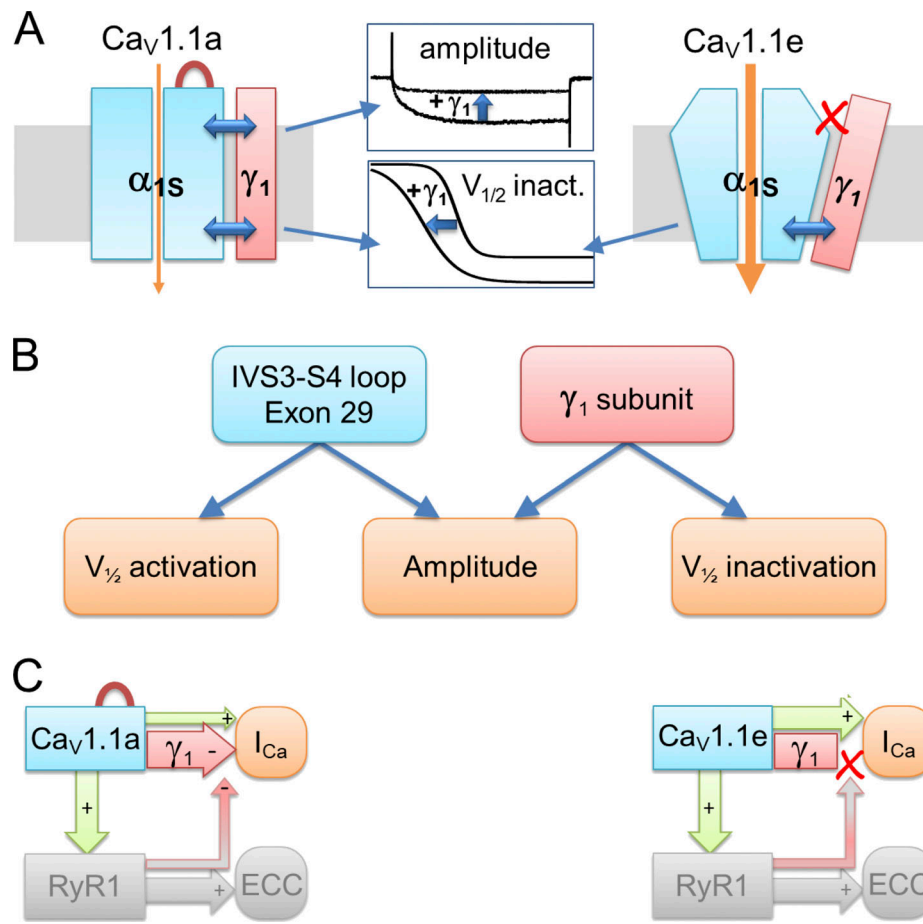


Figure 8. Model of differential γ_1 modulation on $\text{Ca}_V1.1a$ and $\text{Ca}_V1.1e$ currents and its consequences for retrograde coupling. (A) In both $\text{Ca}_V1.1$ splice variants, the γ_1 subunit limits calcium currents by shifting the voltage dependence of inactivation to more hyperpolarizing potentials and rendering inactivation more complete. Inclusion of exon 29 in the extracellular IVS3-S4 loop stabilizes a conformation of the $\text{Ca}_V1.1a$ channel complex, which enables the γ_1 subunit to reduce the current amplitude. (B) The IVS3-S4 loop including exon 29 and the γ_1 subunit require each other for reducing the current amplitude. In contrast, this cooperation is not required to shift the voltage dependence of activation and inactivation, which occurs in a splice variant-dependent manner. (C) In skeletal muscle cells, the negative regulation of calcium currents by the γ_1 subunit is a prerequisite of retrograde current amplification by the RYR1 in $\text{Ca}_V1.1a$ (red arrow from RYR1 to γ_1 ; Grabner et al., 1999; Nakai et al., 1996). Without exon 29 in embryonic $\text{Ca}_V1.1e$, no γ_1 -dependent reduction of current amplitude and no RYR1-dependent relief of this inhibition occurs (Benedetti et al., 2015). The red loop in $\text{Ca}_V1.1a$ indicates inclusion of exon 29.

compared with $\text{Ca}_V1.1a$ is observed with or without γ_1 , and the left-shifted inactivation is observed with or without exon 29, whereas the decreased current amplitude requires their cooperation. Evidently, the interdependence of the analyzed gating properties on the IVS3-S4 loop and the γ_1 subunit is highly specific. Each of the partners independently exerts its specific action on the voltage dependence of activation and inactivation (Fig. 8 B).

Uncoupling of the effects of the γ_1 subunit on current size and inactivation

The finding that the current amplitude of the embryonic variant $\text{Ca}_V1.1e$ is not modulated by the γ_1 subunit, unlike the adult isoform, is surprising. In fact, in a previous study in γ_1 knockout mice, it was reported that the difference in current density between wild type and knockout mice is age dependent, as it was detected only in mice <4 wk of age, but not in older animals (Held et al., 2002). However, this observation cannot be explained by the differential current regulation of $\text{Ca}_V1.1a$ and

$\text{Ca}_V1.1e$ reported here. There is no evidence that primary cultures derived from muscles at different times after birth express different ratios of $\text{Ca}_V1.1e$ and $\text{Ca}_V1.1a$. Moreover, if there were such differences, muscles of mice at ≥ 4 wk would be expected to express predominantly the adult isoform and thus be more susceptible to modulation by γ_1 than younger muscles, not the opposite (Tang et al., 2012; Sultana et al., 2016; Tuluc et al., 2009).

More importantly, unlike the age-dependent reduction in current amplitude, in muscles of γ_1 knockout mice, the shift in the steady-state inactivation was found to be age independent (Held et al., 2002), suggesting that these two functional effects of the γ_1 subunit are not coupled with each other. Here, we observed a similar lack of coupling of the two γ_1 effects in $\text{Ca}_V1.1e$, which is subject to the shift in steady-state inactivation but not to the reduction in current density in cells coexpressing γ_1 . Together, these data strongly suggest that the two γ_1 functional effects are independent of each other and possibly mediated by different domains.

The role of the γ_1 subunit in orthograde and retrograde coupling of $\text{Ca}_v1.1$ and RYR1

The γ_1 subunit was previously demonstrated to be dispensable for EC coupling, i.e., the orthograde coupling between $\text{Ca}_v1.1$ and the RYR1. In fact, in γ_1 -null myotubes, neither the amplitude nor the voltage dependence of the calcium transients was affected (Ahern et al., 2001; Freise et al., 2000). Likewise, calcium release was unaffected in γ_1 -null myotubes, and twitch and tetanic force development of adult γ_1 -null mice was very similar in both fast and slow muscles (Ursu et al., 2001). However, long-lasting potassium-induced contractures were significantly larger, and the shift of the steady-state inactivation in $\text{Ca}_v1.1$ currents was shown to translate into a similar shift in the inactivation curve of calcium release of adult skeletal muscle fibers (Ursu et al., 2004). Our finding that γ_1 equally shifts the voltage dependence of inactivation of $\text{Ca}_v1.1a$ and $\text{Ca}_v1.1e$ indicates that the corresponding shift in the inactivation curve of calcium release also may be present.

In skeletal muscle, not only does $\text{Ca}_v1.1$ activate RYR1, but $\text{Ca}_v1.1a$ calcium currents are also augmented by an interaction of its cytoplasmic II–III loop with the RYR1 (Grabner et al., 1999), a phenomenon termed retrograde coupling. Previously we demonstrated that this function is specific for the adult $\text{Ca}_v1.1a$ splice variant (Benedetti et al., 2015). The currents of $\text{Ca}_v1.1e$ are not reduced when the connection with RYR1 is severed. The dependence of the current augmentation by retrograde coupling on inclusion of exon 29 in the IVS3–S4 loop of $\text{Ca}_v1.1$ mirrors the importance of exon 29 for the current reduction by γ_1 . Based on the results of the earlier study, we had proposed a mechanistic model according to which retrograde coupling partially relieves the inhibition of $\text{Ca}_v1.1$ currents by an unknown, exon 29-dependent factor. Our current study suggests that the γ_1 subunit may be this inhibitory factor. According to this hypothetical model, in the simultaneous presence of exon 29 and the γ_1 subunit, the currents of $\text{Ca}_v1.1a$ are reduced, and this effect is partially counteracted by the interaction with RYR1. If either exon 29 or the γ_1 subunit is missing, this inhibition is absent and there is nothing to be relieved by retrograde coupling (Fig. 8 C).

Conclusions

This analysis of the actions of the γ_1 subunit on the two splice variants of $\text{Ca}_v1.1$ in heterologous cells revealed multiple functions of γ_1 in membrane targeting and functional modulation of the skeletal muscle calcium channel. Interestingly, some of the γ_1 effects are general for both splice variants, while another is specific for the adult $\text{Ca}_v1.1a$. Inclusion of exon 29 in $\text{Ca}_v1.1a$ appears to allosterically render the channel susceptible to the reduction of its currents by γ_1 , as well as to the simultaneous relief of this block by RYR1. Newly generated mammalian cell systems proved highly valuable for this type of coexpression study of $\text{Ca}_v1.1$, but at the same time highlight the multitude of factors involved in shaping the physiological current properties in the native environment of skeletal muscle.

Acknowledgments

Eduardo Ríos served as editor.

We thank Katharina Heinz, Sandra Demetz, Irene Mahlrecht, Nicole Kranebitten, Enikő Török, and Martin Heitz for excellent technical help.

This work was supported by grants from the Tiroler Wissenschaftsfond 2018 (UNI-0404-2238 to M. Campiglio), the Austrian Science Fund (FWF) (T855 and P33776 to M. Campiglio, P30402 to B.E. Flucher, P27809 to J. Striessnig), and the Erika-Cremer habilitation fellowship of the University of Innsbruck to N.J. Ortner. Y. El Ghaleb, M.L. Fernández-Quintero, and W.E. Tuinte are students of the Ca_vX PhD program co-funded by FWF (DOC30) and the Medical University Innsbruck. H.J. Draheim is an employee of Boehringer Ingelheim Pharma GmbH & Co KG.

The authors declare no competing financial interests

Author contributions: M. Campiglio and B.E. Flucher conceived and designed the study. M. Campiglio made the constructs; performed RT-PCR, WB analysis, and flow cytometry staining; and acquired images. N.J. Ortner generated the cell lines and acquired electrophysiological data for the HEK-STAC3 cell line under the supervision of J. Striessnig. Y. El Ghaleb and W.E. Tuinte acquired all the remaining electrophysiological data under the supervision of M. Campiglio, P. Tuluc, and B.E. Flucher. W. Posch and D. Wilflingseder acquired and analyzed the flow cytometry data. M.L. Fernández-Quintero and S. Monteleone performed the modeling under the supervision of K.R. Liedl. H.J. Draheim provided the cell line expressing β_3 and $\alpha_2\delta$ -1. M. Campiglio, and B.E. Flucher wrote the manuscript. All authors contributed to the final draft of the manuscript.

Submitted: 20 September 2021

Accepted: 8 March 2022

References

- Ahern, C.A., P.A. Powers, G.H. Biddlecome, L. Roethe, P. Vallejo, L. Mortenson, C. Strube, K.P. Campbell, R. Coronado, and R.G. Gregg. 2001. Modulation of L-type Ca^{2+} current but not activation of Ca^{2+} release by the γ subunit of the dihydropyridine receptor of skeletal muscle. *BMC Physiol.* 1:8. <https://doi.org/10.1186/1472-6793-1-8>
- Andronache, Z., D. Ursu, S. Lehnert, M. Freichel, V. Flockerzi, and W. Melzer. 2007. The auxiliary subunit gamma 1 of the skeletal muscle L-type Ca^{2+} channel is an endogenous Ca^{2+} antagonist. *Proc. Natl. Acad. Sci. USA.* 104: 17885–17890. <https://doi.org/10.1073/pnas.0704340104>
- Arikkath, J., C.C. Chen, C. Ahern, V. Allamand, J.D. Flanagan, R. Coronado, R.G. Gregg, and K.P. Campbell. 2003. Gamma 1 subunit interactions within the skeletal muscle L-type voltage-gated calcium channels. *J. Biol. Chem.* 278:12112–12119. <https://doi.org/10.1074/jbc.M208689200>
- Armstrong, C.M., F.M. Bezanilla, and P. Horowicz. 1972. Twitches in the presence of ethylene glycol bis-(aminoethyl ether)-N,N-tetracetic acid. *Biochim. Biophys. Acta.* 267:605–608. [https://doi.org/10.1016/0005-2728\(72\)90194-6](https://doi.org/10.1016/0005-2728(72)90194-6)
- Bender, B.J., A. Cisneros 3rd, A.M. Duran, J.A. Finn, D. Fu, A.D. Lokits, B.K. Mueller, A.K. Sangha, M.F. Sauer, A.M. Sevy, et al. 2016. Protocols for molecular modeling with Rosetta3 and RosettaScripts. *Biochemistry.* 55: 4748–4763. <https://doi.org/10.1021/acs.biochem.6b00444>
- Benedetti, B., P. Tuluc, V. Mastrolia, C. Dlaska, and B.E. Flucher. 2015. Physiological and pharmacological modulation of the embryonic skeletal muscle calcium channel splice variant $\text{Ca}_v1.1e$. *Biophys. J.* 108: 1072–1080. <https://doi.org/10.1016/j.bpj.2015.01.026>
- Biel, M., R. Hullin, S. Freundner, D. Singer, N. Dascal, V. Flockerzi, and F. Hofmann. 1991. Tissue-specific expression of high-voltage-activated dihydropyridine-sensitive L-type calcium channels. *Eur. J. Biochem.* 200:81–88. <https://doi.org/10.1111/j.1432-1033.1991.tb21051.x>
- Campiglio, M., and B.E. Flucher. 2017. STAC3 stably interacts through its C1 domain with Ca_v 1.1 in skeletal muscle triads. *Sci. Rep.* 7. 41003. <https://doi.org/10.1038/srep41003>
- Case, D.A., T.A. Darden, T.E. Cheatham, C.L. Simmerling, J. Wang, R.E. Duke, R. Luo, M.R.C.W. Crowley, R.C. Walker, and W. Zhang. 2008. Amber 10. University of California.

- Curtis, B.M., and W.A. Catterall. 1984. Purification of the calcium antagonist receptor of the voltage-sensitive calcium channel from skeletal muscle transverse tubules. *Biochemistry*. 23:2113–2118. <https://doi.org/10.1021/bi00305a001>
- Dayal, A., K. Schrotter, Y. Pan, K. Fohr, W. Melzer, and M. Grabner. 2017. The Ca^{2+} influx through the mammalian skeletal muscle dihydropyridine receptor is irrelevant for muscle performance. *Nat. Commun.* 8:475. <https://doi.org/10.1038/s41467-017>
- Dickson, C.J., B.D. Madej, A.A. Skjevik, R.M. Betz, K. Teigen, I.R. Gould, and R.C. Walker. 2014. Lipid14: The amber lipid force field. *J. Chem. Theor. Comput.* 10:865–879. <https://doi.org/10.1021/ct4010307>
- Fang, K., and H.M. Colecraft. 2011. Mechanism of auxiliary beta-subunit-mediated membrane targeting of L-type ($\text{CaV}1.2$) channels. *J. Physiol.* 589:4437–4455. <https://doi.org/10.1113/jphysiol.2011.214247>
- Flucher, B.E., G.J. Obermair, P. Tuluc, J. Schredelseker, G. Kern, and M. Grabner. 2005. The role of auxiliary dihydropyridine receptor subunits in muscle. *J. Muscle Res. Cell Motil.* 26:1–6. <https://doi.org/10.1007/s10974-005-9000-2>
- Freise, D., B. Held, U. Wissenbach, A. Pfeifer, C. Trost, N. Himmerkus, U. Schweig, M. Freichel, M. Biel, F. Hofmann, et al. 2000. Absence of the gamma subunit of the skeletal muscle dihydropyridine receptor increases L-type Ca^{2+} currents and alters channel inactivation properties. *J. Biol. Chem.* 275:14476–14481. <https://doi.org/10.1074/jbc.275.19.14476>
- Grabner, M., R.T. Dirksen, and K.G. Beam. 1998. Tagging with green fluorescent protein reveals a distinct subcellular distribution of L-type and non-L-type Ca^{2+} channels expressed in dysgenic myotubes. *Proc. Natl. Acad. Sci. USA*. 95:1903–1908. <https://doi.org/10.1073/pnas.95.4.1903>
- Grabner, M., R.T. Dirksen, N. Suda, and K.G. Beam. 1999. The II–III loop of the skeletal muscle dihydropyridine receptor is responsible for the Bi-directional coupling with the ryanodine receptor. *J. Biol. Chem.* 274:21913–21919. <https://doi.org/10.1074/jbc.274.31.21913>
- Gregg, R.G., A. Messing, C. Strube, M. Beurg, R. Moss, M. Behan, M. Sukhareva, S. Haynes, J.A. Powell, R. Coronado, and P.A. Powers. 1996. Absence of the beta subunit (cchb1) of the skeletal muscle dihydropyridine receptor alters expression of the alpha 1 subunit and eliminates excitation-contraction coupling. *Proc. Natl. Acad. Sci. USA*. 93:13961–13966. <https://doi.org/10.1073/pnas.93.24.13961>
- Held, B., D. Freise, M. Freichel, M. Hoth, and V. Flockerzi. 2002. Skeletal muscle L-type Ca^{2+} current modulation in gamma1-deficient and wildtype murine myotubes by the gamma1 subunit and cAMP. *J. Physiol.* 539:459–468. <https://doi.org/10.1113/jphysiol.2001.012745>
- Horstick, E.J., J.W. Linsley, J.J. Dowling, M.A. Hauser, K.K. McDonald, A. Ashley-Koch, L. Saint-Amant, A. Satish, W.W. Cui, W. Zhou, et al. 2013. Stac3 is a component of the excitation-contraction coupling machinery and mutated in Native American myopathy. *Nat. Commun.* 4:1952. <https://doi.org/10.1038/ncomms2952>
- Jay, S.D., S.B. Ellis, A.F. McCue, M.E. Williams, T.S. Vedvick, M.M. Harpold, and K.P. Campbell. 1990. Primary structure of the gamma subunit of the DHP-sensitive calcium channel from skeletal muscle. *Science*. 248:490–492. <https://doi.org/10.1126/science.2158672>
- Jo, S., J.B. Lim, J.B. Klauda, and W. Im. 2009. CHARMM-GUI Membrane Builder for mixed bilayers and its application to yeast membranes. *Biophys. J.* 97:50–58. <https://doi.org/10.1016/j.bpj.2009.04.013>
- Lacerda, A.E., H.S. Kim, P. Ruth, E. Perez-Reyes, V. Flockerzi, F. Hofmann, L. Birnbaumer, and A.M. Brown. 1991. Normalization of current kinetics by interaction between the alpha 1 and beta subunits of the skeletal muscle dihydropyridine-sensitive Ca^{2+} channel. *Nature*. 352:527–530. <https://doi.org/10.1038/352527a0>
- Lee, J., D.S. Patel, J. Stahle, S.J. Park, N.R. Kern, S. Kim, J. Lee, X. Cheng, M.A. Valvano, O. Holst, et al. 2019. CHARMM-GUI membrane builder for complex biological membrane simulations with glycolipids and lipoglycans. *J. Chem. Theor. Comput.* 15:775–786. <https://doi.org/10.1021/acs.jctc.8b01066>
- Nakai, J., R.T. Dirksen, H.T. Nguyen, I.N. Pessah, K.G. Beam, and P.D. Allen. 1996. Enhanced dihydropyridine receptor channel activity in the presence of ryanodine receptor. *Nature*. 380:72–75. <https://doi.org/10.1038/380072a0>
- Nelson, B.R., F. Wu, Y. Liu, D.M. Anderson, J. McAnally, W. Lin, S.C. Cannon, R. Bassel-Duby, and E.N. Olson. 2013. Skeletal muscle-specific T-tubule protein STAC3 mediates voltage-induced Ca^{2+} release and contractility. *Proc. Natl. Acad. Sci. USA*. 110:11881–11886. <https://doi.org/10.1073/pnas.1310571110>
- Niu, J., W. Yang, D.T. Yue, T. Inoue, and M. Ben-Johny. 2018. Duplex signaling by CaM and Stac3 enhances $\text{CaV}1.1$ function and provides insights into congenital myopathy. *J. Gen. Physiol.* 150:1145–1161. <https://doi.org/10.1085/jgp.20182005>
- Obermair, G.J., G. Kugler, S. Baumgartner, P. Tuluc, M. Grabner, and B.E. Flucher. 2005. The Ca^{2+} channel alpha2delta-1 subunit determines Ca^{2+} current kinetics in skeletal muscle but not targeting of alpha1S or excitation-contraction coupling. *J. Biol. Chem.* 280:2229–2237. <https://doi.org/10.1074/jbc.M411501200>
- Polster, A., B.R. Nelson, E.N. Olson, and K.G. Beam. 2016. Stac3 has a direct role in skeletal muscle-type excitation-contraction coupling that is disrupted by a myopathy-causing mutation. *Proc. Natl. Acad. Sci. USA*. 113:10986–10991. <https://doi.org/10.1073/pnas.1612441113>
- Polster, A., S. Perni, H. Bichraoui, and K.G. Beam. 2015. Stac adaptor proteins regulate trafficking and function of muscle and neuronal L-type Ca^{2+} channels. *Proc. Natl. Acad. Sci. USA*. 112:602–606. <https://doi.org/10.1073/pnas.1423113112>
- Rios, E., and G. Brum. 1987. Involvement of dihydropyridine receptors in excitation-contraction coupling in skeletal muscle. *Nature*. 325:717–720. <https://doi.org/10.1038/325717a0>
- Rohl, C.A., C.E. Strauss, K.M. Misura, and D. Baker. 2004. Protein structure prediction using Rosetta. *Methods Enzymol.* 383:66–93. [https://doi.org/10.1016/S0076-6879\(04\)83004-0](https://doi.org/10.1016/S0076-6879(04)83004-0)
- Rufenach, B., D. Christy, B.E. Flucher, J.M. Bui, J. Gsponer, M. Campiglio, and F. Van Petegem. 2020. Multiple sequence variants in STAC3 affect interactions with $\text{CaV}1.1$ and excitation-contraction coupling. *Structure*. 28:922–932.e5. <https://doi.org/10.1016/j.str.2020.05.005>
- Salomon-Ferrer, R., A.W. Gotz, D. Poole, S. Le Grand, and R.C. Walker. 2013. Routine microsecond molecular dynamics simulations with AMBER on GPUs. 2. Explicit solvent particle mesh ewald. *J. Chem. Theor. Comput.* 9:3878–3888. <https://doi.org/10.1021/ct400314y>
- Sandoval, A., J. Arikath, E. Monjaraz, K.P. Campbell, and R. Felix. 2007. gamma1-dependent down-regulation of recombinant voltage-gated Ca^{2+} channels. *Cell Mol Neurobiol.* 27:901–908. <https://doi.org/10.1007/s10571-007s1059210-9>
- Schneider, M.F., and W.K. Chandler. 1973. Voltage dependent charge movement of skeletal muscle: A possible step in excitation-contraction coupling. *Nature*. 242:244–246. <https://doi.org/10.1038/242244a0>
- Schredelseker, J., V. Di Biase, G.J. Obermair, E.T. Felder, B.E. Flucher, C. Franzini-Armstrong, and M. Grabner. 2005. The beta 1a subunit is essential for the assembly of dihydropyridine-receptor arrays in skeletal muscle. *Proc. Natl. Acad. Sci. USA*. 102:17219–17224. <https://doi.org/10.1073/pnas.0508710102>
- Singer, D., M. Biel, I. Lotan, V. Flockerzi, F. Hofmann, and N. Dascal. 1991. The roles of the subunits in the function of the calcium channel. *Science*. 253:1553–1557. <https://doi.org/10.1126/science.1716787>
- Sultana, N., B. Dienes, A. Benedetti, P. Tuluc, P. Szentesi, M. Sztretye, J. Rainer, M.W. Hess, C. Schwarzer, G.J. Obermair, et al. 2016. Restricting calcium currents is required for correct fiber type specification in skeletal muscle. *Development*. 143:1547–1559. <https://doi.org/10.1242/dev.129676>
- Tanabe, T., K.G. Beam, J.A. Powell, and S. Numa. 1988. Restoration of excitation-contraction coupling and slow calcium current in dysgenic muscle by dihydropyridine receptor complementary DNA. *Nature*. 336:134–139. <https://doi.org/10.1038/336134a0>
- Tang, Z.Z., Y. Yarotsky, L. Wei, K. Sobczak, M. Nakamori, K. Eichinger, R.T. Moxley, R.T. Dirksen, and C.A. Thornton. 2012. Muscle weakness in myotonic dystrophy associated with misregulated splicing and altered gating of $\text{CaV}1.1$ calcium channel. *Hum. Mol. Genet.* 21:1312–1324. <https://doi.org/10.1093/hmg/ddr568>
- Tuluc, P., B. Benedetti, P. Coste de Bagneaux, M. Grabner, and B.E. Flucher. 2016. Two distinct voltage-sensing domains control voltage sensitivity and kinetics of current activation in $\text{CaV}1.1$ calcium channels. *J. Gen. Physiol.* 147:437–449. <https://doi.org/10.1085/jgp.201611568>
- Tuluc, P., N. Molenda, B. Schlick, G.J. Obermair, B.E. Flucher, and K. Jurkat-Rott. 2009. A $\text{CaV}1.1$ Ca^{2+} channel splice variant with high conductance and voltage-sensitivity alters EC coupling in developing skeletal muscle. *Biophys. J.* 96:35–44. <https://doi.org/10.1016/j.bpj.2008.09.027>
- Ursu, D., R.P. Schuhmeier, M. Freichel, V. Flockerzi, and W. Melzer. 2004. Altered inactivation of Ca^{2+} current and Ca^{2+} release in mouse muscle fibers deficient in the DHP receptor gamma1 subunit. *J. Gen. Physiol.* 124:605–618. <https://doi.org/10.1085/jgp.200409168>
- Ursu, D., S. Seville, B. Dietze, D. Freise, V. Flockerzi, and W. Melzer. 2001. Excitation-contraction coupling in skeletal muscle of a mouse lacking the dihydropyridine receptor subunit gamma1. *J. Physiol.* 533:367–377. <https://doi.org/10.1111/j.1469-7793.2001.0367a.x>
- Wells, J.A. 1991. Systematic mutational analyses of protein-protein interfaces. *Methods Enzymol.* 202:390–411. [https://doi.org/10.1016/0076-6879\(91\)02020-a](https://doi.org/10.1016/0076-6879(91)02020-a)

- Wu, F., M. Quinonez, M. DiFranco, and S.C. Cannon. 2018. Stac3 enhances expression of human Ca_v1.1 in *Xenopus* oocytes and reveals gating pore currents in HypoPP mutant channels. *J. Gen. Physiol.* 150:475–489. <https://doi.org/10.1085/jgp.201711962>
- Wu, J., Z. Yan, Z. Li, X. Qian, S. Lu, M. Dong, Q. Zhou, and N. Yan. 2016. Structure of the voltage-gated calcium channel Ca_v1.1 at 3.6 Å resolution. *Nature*. 537:191–196. <https://doi.org/10.1038/nature19321>
- Wu, J., Z. Yan, Z. Li, C. Yan, S. Lu, M. Dong, and N. Yan. 2015. Structure of the voltage-gated calcium channel Cav1.1 complex. *Science*. 350:aad2395. <https://doi.org/10.1126/science.aad2395>
- Yang, T., X. Xu, T. Kernan, V. Wu, and H.M. Colecraft. 2010. Rem, a member of the RGC GTPases, inhibits recombinant Ca_v1.2 channels using multiple mechanisms that require distinct conformations of the GTPase. *J. Physiol.* 588:1665–1681. <https://doi.org/10.1113/jphysiol.2010.187203>
- Zamponi, G.W., J. Striessnig, A. Koschak, and A.C. Dolphin. 2015. The physiology, pathology, and pharmacology of voltage-gated calcium channels and their future therapeutic potential. *Pharmacol. Rev.* 67:821–870. <https://doi.org/10.1124/pr.114.009654>

Supplemental material

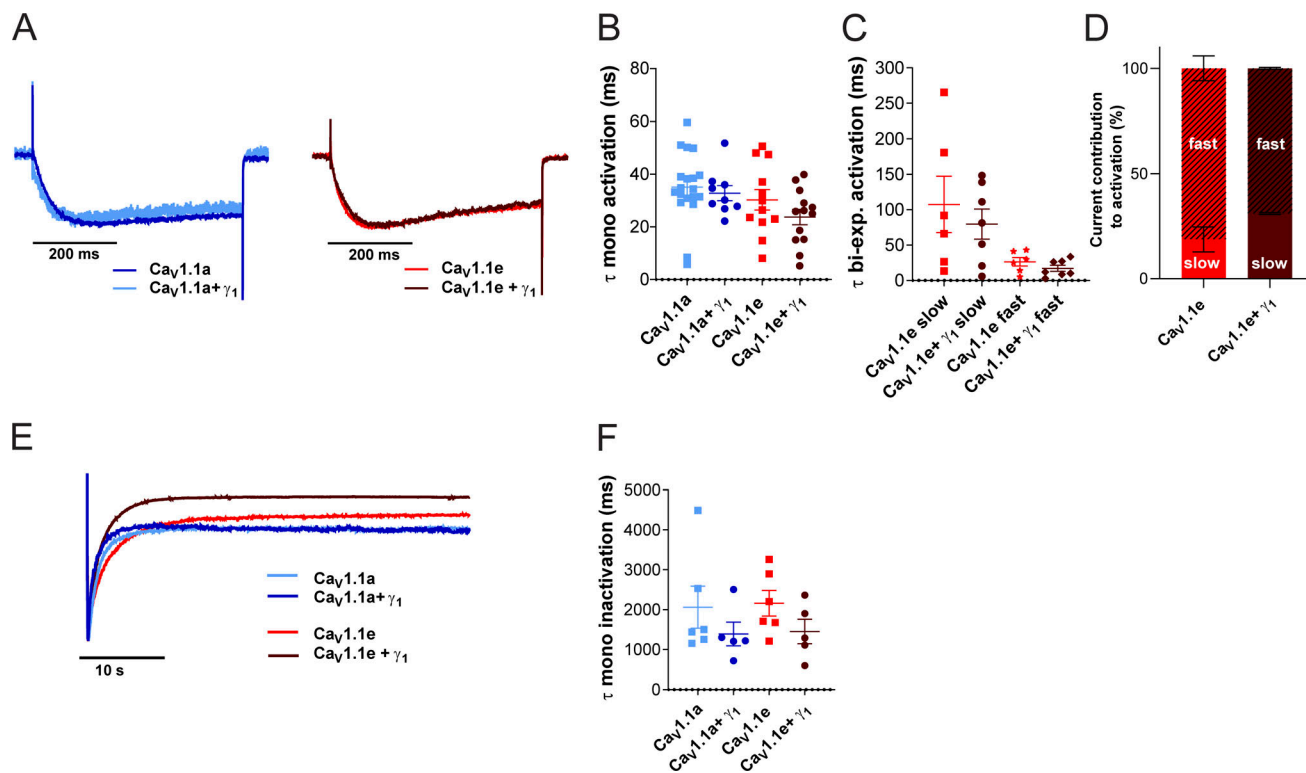


Figure S1. γ_1 Does not affect activation kinetics but shows a trend of accelerated inactivation kinetics. (A–D) Time constants of activation of Cav1.1a (blue, $n = 19$), Cav1.1a + γ_1 (dark blue, $n = 9$), Cav1.1e (red, $n = 12$), and Cav1.1e + γ_1 (dark red, $n = 13$) of a monoexponential and biexponential fit (Cav1.1e) on the rising phase of the inward calcium current during a 500-ms depolarization to V_{max} . (A) Example traces of 500-ms depolarization to V_{max} in Cav1.1a (left) and Cav1.1e (right), normalized to the peak current. (B and C) No differences were found between the time constant of activation of Cav1.1a or Cav1.1e with or without γ_1 coexpression when fitted monoexponentially (B) or between the fast or slow time constant of Cav1.1e ($n = 6$) and Cav1.1e + γ_1 ($n = 7$) of the recordings that could be fitted biexponentially (C); Cav1.1a and Cav1.1a + γ_1 could be fitted only monoexponentially. (D) The current contribution of the fast component was bigger than that of the slow component in both Cav1.1e (slow:fast $\approx 20:80$) and Cav1.1e + γ_1 (slow:fast $\approx 30:70$), but the ratios were similar ($P = 0.41$). (E and F) Time constant of inactivation of Cav1.1a (blue, $n = 6$), Cav1.1a + γ_1 (dark blue, $n = 5$), Cav1.1e (red, $n = 6$), and Cav1.1e + γ_1 (dark red, $n = 5$) of a monoexponential fit on the decay phase of the inward calcium current during a 45-s depolarization to V_{max} . (E) Example traces of 45-s depolarization to V_{max} in Cav1.1a and Cav1.1e, normalized to the peak current. (F) The time constant of inactivation was accelerated by 33% (not significant) when Cav1.1a ($P = 0.32$) or Cav1.1e ($P = 0.15$) was coexpressed with γ_1 . Mean \pm SEM; P values were calculated with Student's t test.